25

Martian polar processes

T. N. TITUS, W. M. CALVIN, H. H. KIEFFER, Y. LANGEVIN, AND T. H. PRETTYMAN

The polar caps are the most active regions on Mars. The annual cycling of atmospheric CO_2 into the seasonal CO_2 ice caps is a driving force of the Martian climate. The polar layered deposits (PLDs), with thousands of layers whose thickness is only resolvable with sub-meter spatial resolution from orbit, may contain a record of past climates. The polar regions contain the majority of known H_2O ice deposits, distributed between the residual caps and near-surface ice in the regolith. In this chapter, we synthesize results from missions and instruments largely presented in detail elsewhere in this book, and consider the implications for Martian polar processes and the areas for future research. The focus here is on presenting evidence for and interpretations concerning the CO_2 cycle and other related polar processes. Implications for water-ice in the subsurface are examined with respect to its effects on the CO_2 cycle. Comparisons of water-ice abundance to the mass and distribution of seasonal CO_2 ice are also explored. While the amount of available data has increased exponentially, our knowledge and understanding of Martian polar processes has increased much more gradually. As each question about the polar regions of Mars is answered, several new questions are brought to light. Many of the processes that occur in the polar regions of Mars do not have direct analogs on Earth, but do have analogs in other parts of the Solar System. If we are to understand the history of Mars, and by association, the evolution of Earth within our Solar System, we must understand the polar regions. We conclude the chapter with a review of those questions that have at least been partially answered since 1992, as well as those questions where the answers still elude us.

25.1 INTRODUCTION

25.1.1 Historical overview

The history of Mars polar cap observations through the Viking era, with the now well-known seasonal deposition of CO_2 ice, is summarized in *Mars*, the University of Arizona Press book, in chapters by James *et al.*, (1992) and Jakosky and Haberle (1992). Briefly, a long history of telescopic observations of the polar regions of Mars showed that the seasonal cycle, as expressed by the location of the cap edge, closely repeats from year to year. The caps were assumed to be water ice until shortly before the era of spacecraft observations. Prediction that the CO_2 atmosphere should condense in the winter (Leighton and Murray, 1966) was confirmed by Mariner 7 infrared spectrometer observations that recorded the appearance of forbidden transitions of CO_2 ice (Herr and Pimentel, 1969) and telescopic spectral observations by Larson and Fink (1972). It is this process of the CO_2 atmosphere condensing out as snow and ice onto the surface during autumn and winter and then subliming back into the atmosphere in the spring that drives the current Martian climate. Roughly 25% of the atmosphere, which is 95% CO_2 by volume, is cycled through the seasonal caps annually (Tillman *et al.*, 1993; Forget and Pollack, 1996; Kelly *et al.*, 2006). This CO_2 cycle dominates atmospheric circulation on Mars and must be thoroughly understood before the fundamental questions about Mars' climate history and the global distribution of near-surface water can be addressed.

25.1.2 Nomenclature

As observations of Mars expand to higher spatial resolutions and to a wider range of data types (e.g., radar, neutrons, gamma rays), conflicting or vague terminology may lead to confusion with regard to surface features and phenomena. Throughout this chapter, we will use the commonly used nomenclature and terminology as laid out by the US Geological Survey (Herkenhoff *et al.*, 2006), in which seasonal deposits overlie residual or permanent ice. In both the northern and southern hemispheres, layered deposits, which include nonice materials, underlie the icy caps and separate them from the surrounding plains.

25.2 THE POLAR ENERGY BALANCE

The amount, rate, and distribution of CO_2 condensation/sublimation is determined by the balance of several energy sources and sinks, including insolation (exposure to sunlight), net radiative loss to space, the latent heat of fusion, summertime heat storage in the regolith, and atmospheric storage and transport of energy. Mars climate models attempt to replicate this energy balance through a variety of physical processes. For recent summaries and detailed physical descriptions, see Pollack *et al.* (1993), Hourdin *et al.* (1995), and Forget *et al.* (1998, 1999). We only briefly

The Martian Surface: Composition, Mineralogy, and Physical Properties, ed. Jim Bell. Published by Cambridge University Press.

summarize the various contributions to the energy balance here.

25.2.1 Albedo effects and feedback

Surface albedo is inversely proportional to energy absorbed; hence, sublimation depends on surface processes such as ice grain size, water and dust contamination, and photometric effects (solar illumination and surface scattering function). As a general rule, the seasonal caps are brighter in late spring than they are in early spring. This is true for both the northern and the southern caps, with the notable exception of the so-called "cryptic region" (discussed in Section 5.3 below) located within the southern seasonal cap (Kieffer *et al*., 2000). Possible causes include seasonal brightening with increased solar insolation (and other photometric effects), and cold trapping of water vapor into frost (Paige, 1985; Houben *et al*., 1997). The North Polar Region is generally richer in water ice than the South Polar Region; migration of H_2O is observed along the edge of the retreating northern seasonal cap (Kieffer and Titus, 2001; Schmitt *et al*., 2005a,b; Titus, 2005a; Wagstaff *et al*., 2007). While the Mars Express Observatoire pour la Minéralogie, l'Eau, les Glaces et l'Activité (OMEGA) near-infrared (NIR) imaging spectrometer observed H_2O as a component of the southern retreating seasonal cap (e.g., Langevin *et al*., 2005), those observations do not reveal large scale H_2O ice lags on the edge of the cap. Possible ice lags are seen at the end of the southern cap retreat, but these could also be an artifact of subpixel mixing of remnant CO_2 ice and dust (Titus, 2005b; Douté *et al*., 2007). The third possible process, photometric effects, has not been fully explored. For most studies, CO_2 ice has simply been assumed to be Lambertian (Paige, 1985; Paige and Ingersoll, 1985; James *et al*., 2005).

25.2.2 Atmospheric effects, clouds, and surface emissivity

In addition to surface albedo, the temperatures observed by orbiting spacecraft reflect surface temperature, surface emissivity, and the atmospheric temperature and opacity profiles. A hot and dusty or warm and cloudy atmosphere will increase both the radiative losses to space as well as increase the downwelling radiation on the surface. During the polar night, when the insolation is zero, both surface emissivity and atmospheric opacity can significantly modify the energy budget. The primary factors that influence surface emissivity are CO_2 grain size and purity. The major influence from the atmosphere is that an increase in aerosol opacity can reduce the radiative losses to space.

Results from the Mars Global Surveyor (MGS) Mars Orbiter Laser Altimeter (MOLA; Neumann *et al*., 2003), Thermal Emission Spectrometer (TES; Pearl *et al*., 2001), and Radio Science experiments (Tyler *et al*., 2001; Hinson and Wilson, 2002) all indicate that there is significant CO_2 cloud cover during the polar night at both poles. Much of the cloud cover is in the form of dust-free haze, often with a component of H_2O ice, as opposed to stratified clouds (Pearl *et al*., 2001). Supercooled conditions can arise, causing instability and strong convection currents (Colaprete *et al*., 2007). The exact effects of this process on the energy balance are still poorly constrained. Nonetheless, these new observations do provide a context for many previous observations, dating back to the first spacecraft to observe the polar night.

Early spacecraft observations of the polar regions revealed brightness temperatures significantly lower than the expected kinetic temperature ($\sim$140 K) for CO_2 ice in equilibrium with a CO_2 atmosphere (Kieffer *et al*., 1976). These cold areas or cold spots were typically a few hundred kilometers in diameter, with 20 μm brightness temperatures as low as 130 K and typical lifetime of a few days (Kieffer *et al*., 1976). Plausible suggestions for the cause of the cold spots included high-altitude CO_2 clouds (Hunt, 1980), surface CO_2 snow, and low partial pressures of CO_2. Hess (1979) showed that low partial pressure (i.e., an increase in the mixing ratio of inert gases) at the surface was dynamically unstable and would mix to the top of the atmosphere. Forget *et al*. (1995) were able to fit Mariner 9 IRIS spectra with a combination of fine-grained CO_2 snow and a thin layer of warmer water clouds. They suggested that the cold spots were freshly deposited CO_2 snow or perhaps CO_2 condensates high in the atmosphere. More recently, instruments on board MGS, Mars Odyssey, and Mars Express have all observed high-altitude clouds (Ivanov and Muhleman, 2001; Montmessin *et al*., 2006). While a small fraction of the cold spots could be "dry-ice blizzards" in progress, these snow storms are short-lived, perhaps only a few hours. Condensation models instead suggest that most of the cold spots observed are the result of surface emissivity effects that appear to be a result of these storms (Hansen, 1999; Titus *et al*., 2001). Because the snow that remains once the storms pass can be observed as cold spots for up to several weeks, they can affect the long-term energy balance within the polar night.

25.2.3 Regolith and near-surface ice

Most energy balance studies have followed the example of Leighton and Murray (1966) and ignored the contribution of the regolith (e.g., Kieffer *et al*., 2000). The discovery of high concentrations of near-surface H_2O ice at high latitudes (see Chapters 5 and 6) has brought into question this assumption. Studies (e.g., Paige and Ingersoll, 1985; Haberle *et al*., 2004; Kieffer, 2007) have shown that the energy balance, and thus the accumulation of seasonal CO_2, can be greatly affected by the presence of ice. H_2O ice can strongly influence the surface thermal inertia (see Chapter 18), delaying the formation of seasonal CO_2 frost and reducing net accumulation.

25.2.4 Atmospheric transport

The final contribution to the atmosphere energy balance discussed here is heat capacity and lateral transport. The heat capacity of the atmosphere is small, and thus its contribution can generally be neglected. However, the lateral transport of heat is not well constrained and could be quite large, depending on the location and season. For example, a study by Haberle *et al*. (2004) suggests that the atmospheric

transport contribution may be the same order of magnitude as the heat storage contribution from an icy regolith.

A quantitative analysis of the abundance of noncondensable gases has been carried out by Prettyman *et al*. (2004) using neutron spectroscopy (thermal-and epithermal-counting data) and by Sprague *et al*. (2004) using gamma ray spectroscopy. The abundance of noncondensable gases increases rapidly as CO_2 is deposited at high latitudes. This is likely the result of the formation of a strong polar vortex accompanying the condensation flow and inhibiting meridional mixing of the polar atmosphere with lower latitudes. The magnitude of the enrichment observed during the advance was used to estimate coefficients for eddy diffusion by Sprague *et al*. (2004). During the recession, CO_2 subliming from the cap mixes with the atmosphere, resulting in depletion of noncondensable gases. While one of the early hypotheses of cold spot formation was the reduction of the CO_2 partial pressure (or an increase in the mixing ratio of inert gases like Ar), the observed enhancement of Ar (approximately a factor of 6 in the south) is only sufficient to depress the CO_2 frost temperature by $\sim 2^\circ$. The effects of inert gas enrichments in the north are even smaller, due to a weaker polar vortex. Observations such as these, along with additional modeling, may provide insights and constraints on atmospheric dynamics and transport.

25.3 SPECTRAL PROPERTIES OF MARTIAN ICES

As described in Chapter 2, both water and CO_2 ice have strongly varying spectroscopic properties with wavelength. Small amounts of water or dust in CO_2 ice can dramatically change the reflectivity and emissivity, thus modifying the energy balance of the seasonal frost cap.

The optical constants for CO_2 ice have been measured over the solar reflectance and thermal emission ranges by Hansen (1997, 2005), and measurements of the strong lines have been made by Quirico and Schmitt (1997). Laboratory measures of the spectral properties of H_2O over a wide wavelength range were compiled by Warren (1984), and important spectral variations with temperature were measured by Grundy and Schmitt (1998). In addition, optical constants for Martian dust have been derived from both down-looking satellite observations (Clancy *et al*., 1995; Clancy *et al*., 2003; Wolff and Clancy, 2003; Wolff *et al*., 2006) and landed observations of both the surface and atmosphere (Pollack *et al*., 1995; Ockert-Bell *et al*., 1997; Markiewicz *et al*., 1999; Tomasko *et al*., 1999; Bell *et al*., 2000; Lemmon *et al*., 2004). While these dust spectral shapes appears to be adequate for modeling dirty ice deposits, one must be careful. For example, there is an order of magnitude difference between the VIS/NIR (VIS – Visible Imaging Subsystem) optical constants of Lemmon *et al*. (2004) and the commonly used optical constants of Clancy *et al*. (1995). Nonetheless, many spectral modeling efforts have taken advantage of these recently derived optical constants, combined with modern scattering models (Hapke, Mie, delta-Eddington), and the models often match well with observations (e.g., Calvin, 1990; Grundy *et al*., 1999; Kieffer *et al*., 2000; Glenar *et al*., 2005; Hansen *et al*., 2005; Langevin *et al*., 2006).

Example spectra of CO_2 ice, H_2O ice, dust, and mixtures of these components are shown in Figures 25.1 and 25.2. Particle scattering properties were computed from Mie theory (intimate mixtures), and the surface reflectance was computed using a two-stream delta-Eddington model (Kieffer *et al*., 2000). Pure CO_2 has low absorption coefficients in the solar reflected wavelength region, so that small amounts of H_2O or dust have a large effect on the reflectance. For example, in the 1.5–2.5 μm region, only 0.1% fine dust or 1% fine H_2O will lower the reflectance about 25%; at visible wavelengths only dust can darken CO_2 frosts. In the thermal IR, CO_2 grain size has a large effect on emissivity. For example, fine dust (typical atmospheric-particle sized) at the 0.1% level will raise the emissivity in the 25 μm band to 0.85, and sand-sized (0.25 mm) particles of either rock or H_2O can dominate the spectrum of coarse-grained CO_2.

Both the OMEGA instrument and the Compact Reconnaissance Imaging Spectrometer for Mars (CRISM) on the Mars Reconnaissance Orbiter observe these polar deposits in the wavelength range where multiple, diagnostic features can separate H_2O and CO_2 ices. Initial analyses have shown evidence for the evolution of water frost grain size in the residual ice cap (Langevin *et al*., 2005) and allow the determination of effective grain size and level of ice and dust contamination. Using the full spectral capabilities of these instruments is an area of active research and study that has only just begun.

25.4 ACTIVE PROCESSES: THE ANNUAL CYCLE

Because the Martian atmosphere is so thin, its heat capacity and thermal-transport capability compared to the Earth's atmosphere and ocean is miniscule. That fact and the planet's greater distance from the Sun result in the cooling of the Martian winter atmosphere to its condensation point. The resulting condensation of CO_2 near the poles (in seasonal amounts up to six times the columnar mass of the atmosphere) drives a net CO_2 circulation, with concomitant zonal transport of H_2O and dust. The result of a full annual cycle is quite different for these three materials: CO_2 processes are reversible and the cycle is virtually closed; H_2O and dust can form condensation nuclei for CO_2 and be carried into the seasonal cap; H_2O returns to the vapor state and becomes mobile after all the CO_2 is gone. Dust probably becomes partially trapped and is included in the PLDs by as-yet unknown processes. The CO_2 condensation rates and the transport of H_2O and dust are becoming treated by increasingly competent and complex General Circulation Models (GCMs).

There is the potential for many positive and negative feedback processes in these annual cycles (some of which we discuss here). Presumably, natural processes would drive

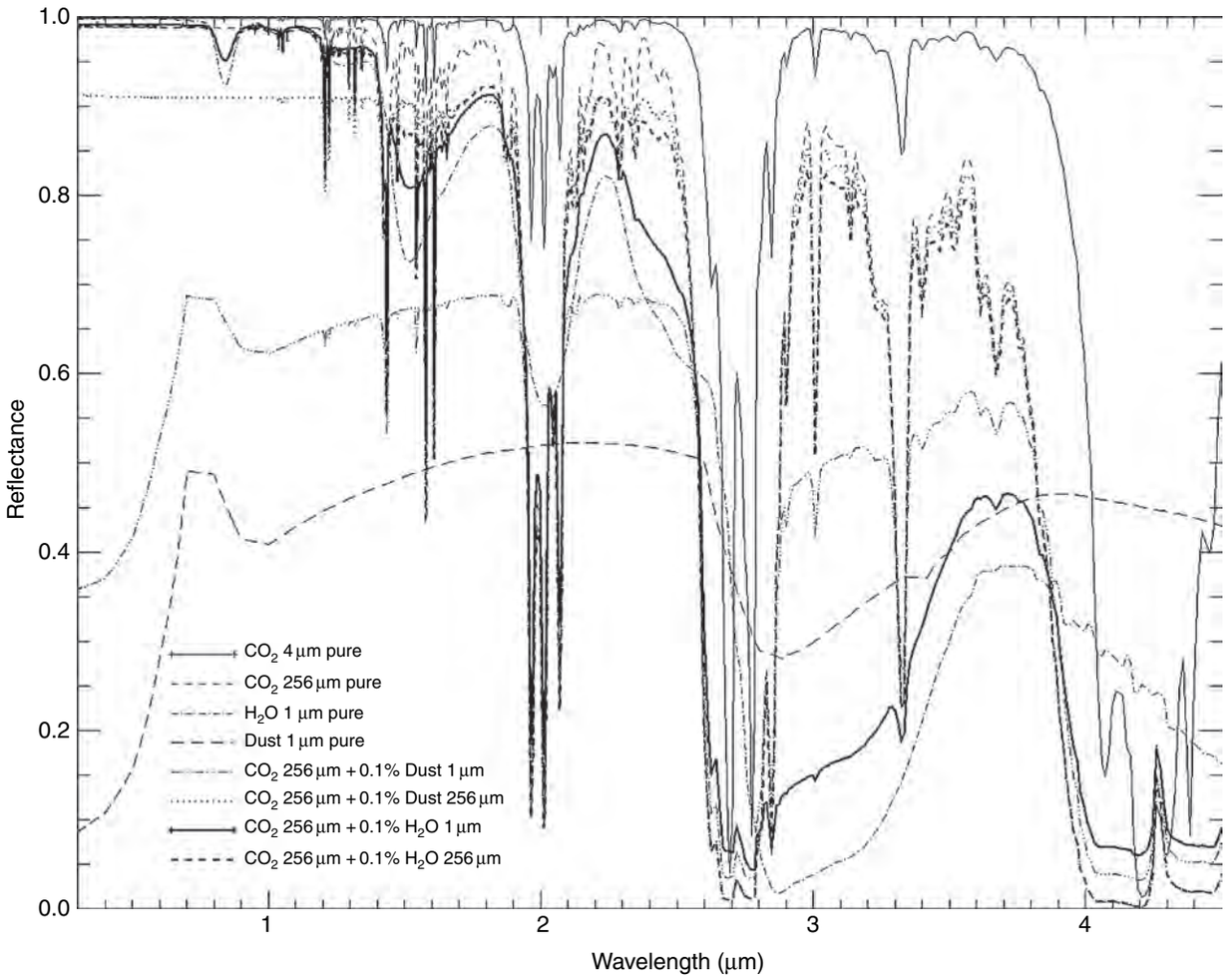

Figure 25.1. Computed spectra of polar ice components and mixtures, in the solar reflected wavelength region. Values are the Bond albedo for thick materials computed using Mie theory and a delta-Eddington radiative transfer model. Complex indices of refractions for CO_2 ice are based on Hansen (1997, 2005); for H_2O on Warren (1984), with the near-IR replaced with the temperature-dependent measurements of Grundy and Schmitt (1998) at 190 K and for dust (Wolff *et al.*, 2006). The solar incidence angle was set to 60°. The compositions, minor mass fractions, and grain radii in μm are listed in the legend. Pure CO_2 is shown for grain radii of 4 and 256 μm; pure H_2O and pure dust each are for radii of 1 μm, representative of atmospheric values. The large effects of admixtures of 0.1% (by mass) dust and H_2O of these size aerosols are shown for 256 μm-sized grains of CO_2. The effects for larger grains of dust and H_2O are considerably less at the same mass fractions.

Mars to a state where these all balance and the net effect of a mean annual cycle is virtually zero. However, the presence of major changes in the insolation cycle due to periodic changes in Mars spin orientation and orbital parameters (e.g., Ward and Rudy, 1991) may result in a continuing imbalance. It is difficult for us to estimate the magnitude of this imbalance because although we know the period and magnitude of the driving insolation variations (at least for the last few million years), we know little about the timescales of the equilibrating processes.

Given the finely layered appearance of the PLDs, the large exchange of carbon dioxide between the atmosphere and the seasonal caps, and the known presence of water in both seasonal and residual caps, three major components appear to control the current Martian climate and have influenced the formation and evolution of the ice caps and their underlying layered terrains. These are the carbon dioxide, water, and dust cycles. These are often treated separately in GCMs, but all contribute to evolution of the polar regions as observed. While we will not explicitly discuss the dust cycle in this chapter, the reader should be aware that the dust cycle impacts the polar regions by changing the albedo and emissivity of CO_2 ice and by changing the energy balance of the planet by scattering solar insolation back into space during global and regional dust storms. Also, some of the dust that is incorporated into the seasonal caps may eventually become part of the PLDs. For more summaries and details about the dust cycle, see Kahn *et al.* (1992), Basu *et al.* (2004), and Kahre *et al.* (2006).

25.4.1 CO_2 transport

Mars' northern and southern seasonal polar caps are formed during their respective autumn and winter seasons both by

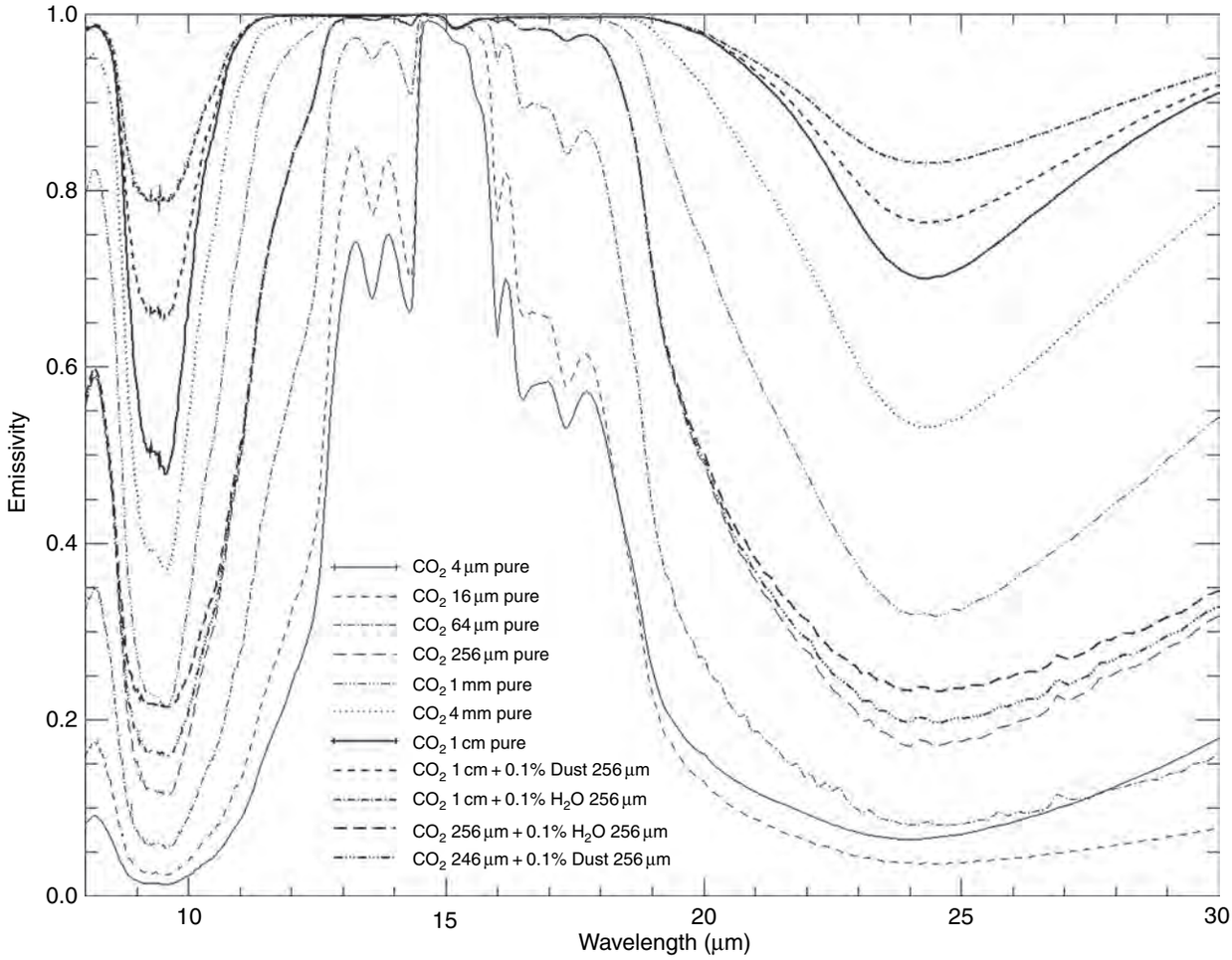

Figure 25.2. Computed spectra of polar ice components and mixtures in the thermal emission wavelength region. Values are the zenith emissivity (1 – Bond albedo); otherwise conditions are as stated in Figure 25.1. The progression of the 25 μm band as a function of grain size is shown for pure CO_2; the similar feature at 9.5 μm is difficult to utilize on Mars because of the strong spectral absorption of dust in the atmosphere. The effect of admixtures of 0.1% (by mass) dust and H_2O are shown for 1 cm-sized CO_2 (uppermost three curves: top is with H_2O, middle is with dust, bottom is pure CO_2); the three curves with minima near 0.2 that converge on both sides of the strong CO_2 bands near 15 μm show the effect of the same admixtures for CO_2 grain sizes of 256 μm.

condensation of atmospheric CO_2 directly onto the surface and through atmospheric precipitation in the form of CO_2 snow. During the polar spring and summer, the seasonal ice sublimes, returning CO_2 to the atmosphere. James *et al.* (1992) summarized the seasonal flow of carbon dioxide between the North and South Polar caps based mainly on Mariner and Viking data. Considerable amounts of new data from MGS, Mars Odyssey, and Mars Express have added to our understanding of the CO_2 cycle, which is discussed in Section 25.5.

25.4.2 H_2O transport

Water is currently known to reside in the residual ice caps, at shallow depth in the regolith, and in the atmosphere. Among the major unresolved questions is the exchange of water between these reservoirs; what amounts and timescales are involved? Water is known to occur as both vapor and ice clouds (e.g., Jakosky, 1985), and was seen to condense at lower latitudes at the Viking landing site (Jones *et al.*, 1979; Wall, 1981; Svitek and Murray, 1990). An annulus of water ice follows the retreat of the northern seasonal cap (Kieffer and Titus, 2001; Langevin *et al.*, 2006), and water-ice lags may also persist after the retreat of CO_2 frost in the south (Titus, 2005b). Water ice at the edges of the re-entrant valleys of the south residual cap has been mapped by OMEGA (Bibring *et al.*, 2004). Water-ice clouds form the North Polar hood, which can extend as far south as 48° N (Zasova *et al.*, 2005) and can begin to obscure the residual cap as early as $L_s \sim 167°$ (L_s is the heliocentric longitude of Mars in its orbit measured from Vernal Equinox; Wang and Ingersoll, 2002) with the onset of seasonal CO_2 frost deposition. Clouds and other weather are seen to form repeatable patterns from year to year (Cantor *et al.*, 2002).

Smith (2002) presented the MGS-TES view of water vapor in the atmosphere. Peak atmospheric water vapor is noted in the north at $L_s \sim 120°$, with consistent values over two Martian northern summers. In contrast, water over the southern cap is highly variable (as seen by Smith [2004], and inferred from earlier observations [Barker *et al.*, 1970; AQ1

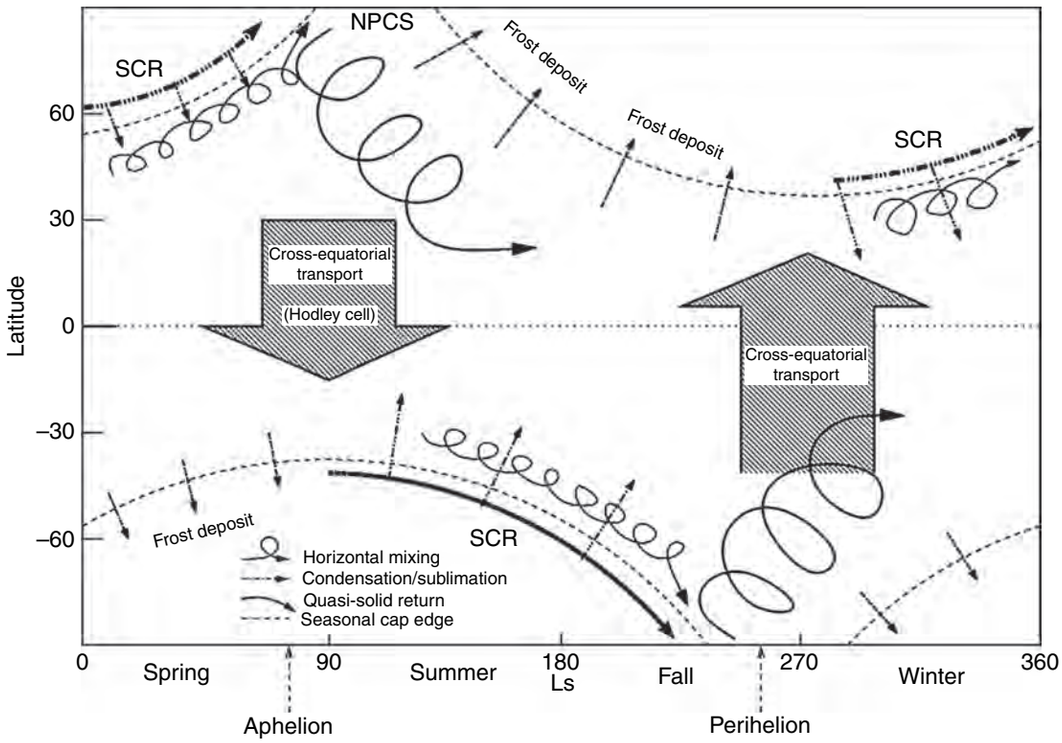

Figure 25.3. The components of the H_2O cycle, including the migration of H_2O ice along the edge of the retreating seasonal caps (Montmessin *et al*., 2004).

Jakosky and Haberle, 1990; Titov, 2002]). This suggests that a water cap underlies the residual CO_2 ice in the south, with a highly variable history of exposure and sublimation. Models suggest that the amount of water sublimated from the north residual cap is insufficient to account for the peak amounts seen in the atmosphere (100 precipitable μm in the north and 50 precipitable μm in the south), and that regolith exchange must also contribute to the observed atmospheric reservoir in the northern summer (Jakosky, 1983a,b; Jakosky *et al*., 1997). The Mars Odyssey Gamma Ray Spectrometer/Neutron Spectrometer (GRS/NS) results have been interpreted to indicate a vast mid- to high-latitude subsurface reservoir of ice-permeated ground, supporting this view (Boynton *et al*., 2002; Feldman *et al*., 2004; see also Chapters 5 and 6), yet the amount of ice actively in exchange with the atmosphere has not been well constrained. While GRS/NS results show large amounts of subsurface ice in both the north and the south, the fact that the southern hemisphere lacks a large water-vapor peak implies that the ground ice in the southern hemisphere is not in exchange with the atmosphere and may thus be more deeply buried, as inferred from thermal inertia data (Paige *et al*., 1994).

General Circulation Models have been used extensively to understand the water cycle, especially the role of clouds, which can impact the radiation budget of the planet (e.g., Houben *et al*., 1997; Richardson and Wilson, 2002; Montmessin *et al*., 2004; see Figure 25.3). Recently, Tyler and Barnes (2005) have used a high resolution GCM to model water transport and winds in the North Polar Region, noting eddies consistent with repeated cloud patterns observed by the Mars Orbiter Camera (MOC) on MGS, and strong circulation variability with season during the northern summer. They note a "storm track" linking the polar regions with Tharsis Montes and Alba Patera, suggesting that this corridor may be responsible for transport of water away from the pole, and supporting the observation of Smith (2002) that water from the north crosses the equator as the seasonal vapor maximum decays.

25.5 SEASONAL SURFACE DEPOSITS

The growth and recession of the seasonal caps are the most dynamic processes on Mars and were first recorded in the drawings of Cassini in 1666. In the late eighteenth century, Herschel (1784) was the first to observe the dynamic nature of the polar caps and believed that the polar caps were composed of H_2O; this was the popular belief for almost two centuries. Near the end of the nineteenth century, there were a few dissenters. For example, A.C. Ranyard and G.J. Stoney believed that Mars was too small to gravitationally hold onto H_2O. They believed that the polar caps must be dry ice, not wet ice (e.g., Stoney, 1898). It was not until 1966 that Leighton and Murray (1966) determined from models and observations of surface temperatures and pressures that the seasonal caps must be composed of CO_2. Even then, the idea that the polar caps were composed of anything besides H_2O ice was not popular (Bruce Murray, 2006, pers. comm.). Mariners 6 and 7 flew past Mars in 1969 and firmly established that the surface temperatures of the seasonal caps were indeed consistent with the presence of CO_2 ice (Neugebauer *et al*., 1971).

Just as terrestrial oceans control the climate on Earth, the seasonal polar caps control the climate on Mars, with 25% of the atmosphere being cycled from vapor to ice and back to vapor annually (Tillman *et al.*, 1993). While there seems to be little annual variation of global properties (e.g., atmospheric pressure), there are regional and local variations in the cap's recession (e.g., James *et al.*, 1992; Bonev *et al.*, 2002). Global dust storms do not appear to have a major impact on the global rate at which the polar caps advance and recede, but apparently they can affect regional and local rates of CO_2 condensation and sublimation, such as an early disappearance of the "Mountains of Mitchel" (e.g., James *et al.*, 1992; Martin *et al.*, 1992).

25.5.1 Seasonal cap edges

The most observable parameter that describes the polar seasonal caps is their size. The size of the caps has been measured since the days of Herschel. Telescopic observations of the dynamic nature of the seasonal caps have been restricted to the recession phase of the caps, however. During the period of growth, Mars is tilted away from the Earth, thus placing the cap edge at unfavorable viewing angles. In addition, the cap edge is close to the terminator and is often obscured by clouds or haze. Fischbacher *et al.* (1969) compiled recession curves for the polar caps from 1905 to 1965, using photographic material archived at the Lowell Observatory. A number of other observers used telescopic data to characterize the cap recessions in the early 1960s through the present. Spacecraft observations began in 1969 with Mariner 7 and continue to the present day. A compilation of both telescopic and spacecraft observations of the polar caps can be found in James *et al.* (1992), Hansen (1999), and Benson and James (2005).

The advance and retreat of the polar cap from year to year may contain many clues to help elucidate little understood physical processes. For example, summertime heat storage in the regolith could delay the onset of the seasonal CO_2 cap. The onset of the seasonal cap could also be directly affected by the thermal inertia of the near-surface regolith and place constraints on the depth of the ice table.

Parameterizations of the seasonal cap edges provide useful constraints on atmospheric GCMs and mesoscale models. Longitudinally resolving the cap edges as they advance and retreat constrains the times when zonal means are appropriate and when longitudinal asymmetries make zonal means invalid. Figure 25.4 illustrates one such parameterization, where both the advance and the retreat of the seasonal caps have been modeled as a series of sines and cosines. These same kinds of parameterizations can also be used when modeling other data that have large spatial resolutions, such as GRS and NS data. By knowing where the cap edge should be, coarse spatial resolution instruments can correct for subpixel mixing caused by their large instrument point spread functions convolving both frosted and frost-free areas.

Northern seasonal cap edge

The northern seasonal cap has been less well studied than the south, both because Mars is typically farther from Earth

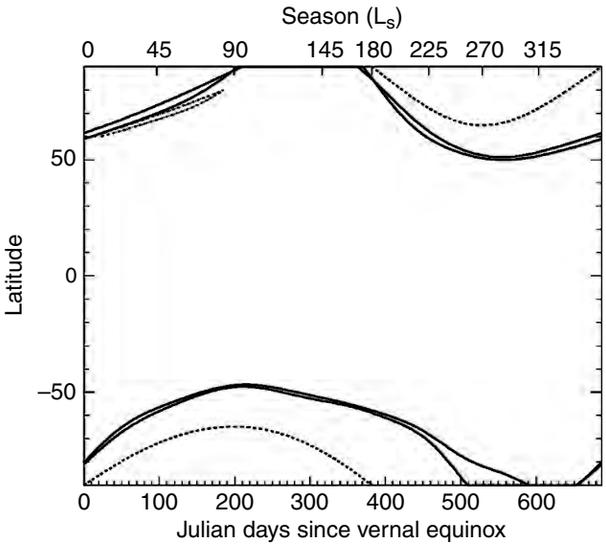

Figure 25.4. Polar cap edge behavior. The red lines indicate the best-fit sine-cosine function for the northern cap edge at 0° E, 180° E and the southern cap edge at 45° E, 135° E. The dotted black line is the subsolar latitude and the two solid black lines are the edge of polar night. The blue line indicates the edge of the visual cap at 0° E and 180° E.

during Martian northern winter and due to the consistent formation of the North "Polar hood." The north cap exhibits a near-symmetric retreat, which has been well characterized at visible wavelengths by both telescopic and spacecraft observations. However, the advance of the cap has not been well characterized until recently. Kieffer and Titus (2001) have used zonal means to observe surface temperature and visible bolometric albedo with season using MGS TES. The TES thermal observations show a nearly perfect symmetric advance; that is, condensation at consistent latitude across all longitudes, with the most northern edge of the seasonal cap occurring between longitudes 245° E and 265° E and the most southern edge of the seasonal cap occurring between 280° E and 30° E (Titus, 2005a). The advance of the northern cap typically leads the advance of the edge of polar night by 10° of latitude (Figure 25.3). The northern spring retreat is also nearly symmetric in both visual and thermal observations, and follows the same small asymmetries as seen in the advance. The latitude difference between the maximum and minimum extent of the thermal cap is generally between 3° and 5°, regardless of whether the cap is advancing or retreating. Benson and James (2005) saw changes in the recession rates between 2000 and 2002. The changes occurred in the same longitude ranges as Titus (2005a) saw the asymmetries, with the slower retreat occurring between longitudes 300° E and 30° E and the faster retreat between 230° E and 270° E.

In addition to four Martian years of seasonal observations by TES and MOC, the north seasonal cap was observed in detail with OMEGA in 2004 and 2006. The bright ring at intermediate temperatures (~180 K) observed by TES (Kieffer and Titus, 2001) in early spring is confirmed by OMEGA as resulting from H_2O ice frost, with a sublimation front which lags by up to 4° in latitude south of the CO_2 ice sublimation front. H_2O ice contamination of CO_2

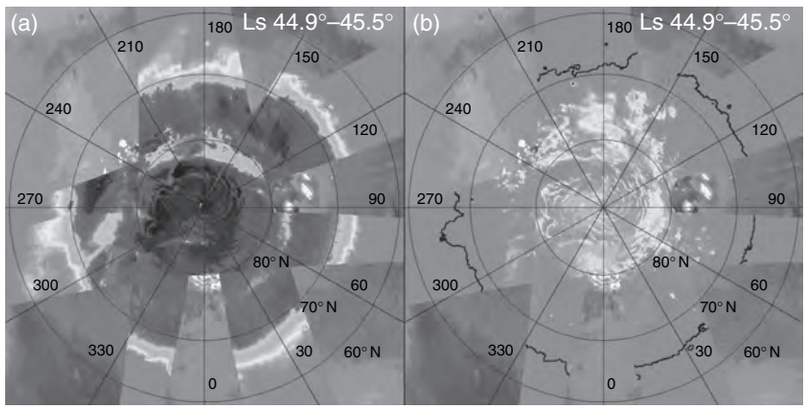

Figure 25.5. Spatial distribution of spectral signatures of CO_2 ice and H_2O ice observed by OMEGA in mid northern spring (L_s ~45°, April 2006). (a) band depth of the H_2O ice absorption feature at 1.5 μm. The grayscale covers the range from 60% (black) to 0% (white). Weak signatures between 60° N and 70° N correspond to water ice clouds; (b) band depth of the CO_2 ice absorption feature at 1.43 μm, also from 60% (black) to 0% (white). The black outline corresponds to the boundary of regions with strong H_2O ice signatures. At this season, H_2O ice dominates the spectral signature of the northern seasonal cap, except for a few regions where strong spectral signatures of CO_2 ice are still observed. (For a color version of this figure, please refer to the color plate section or to the online e-Book version of this chapter.)

ice is ubiquitous in the northern seasonal cap at all stages of its evolution. H_2O ice dominates the spectral signatures over most of the seasonal cap after mid-spring (L_s ~45, see Figure 25.5).

In addition to the presence of an H_2O ice annulus that tracks the seasonal cap retreat, occasional brightening of the entire seasonal cap will occur (Kieffer and Titus, 2001). This temporary brightening of the cap (referred to as "flashing") typically lasts for a day, and then returns to normal. This type of flashing is most likely due to a sudden cold trapping of water vapor across the entire cap, resulting in a thin and temporary layer of bright water frost. This relatively slow type of flashing should not be confused with the "flashing" observed by many amateur astronomers (e.g., Wilson, 1937; Wells and Hale, 1971; Haas, 2003), which occurs very quickly and is probably the reflection of sunlight off of ice crystals in high-altitude Martian clouds, or possibly specular reflections off of isolated pockets of surface ice.

South polar seasonal cap edge

During the southern fall, the advance of the southern seasonal cap is nearly symmetric, just as in the case of the northern seasonal cap. Only a 2°–4° difference in the latitude of the cap edge has been observed, with the most northern extension generally occurring near longitude 300° E. This symmetry remains until L_s ~220°, which corresponds to the season when the cryptic region (Section 25.5.3) has maximum albedo contrast with the rest of the seasonal cap.

The retreat of the southern cap has been known to be asymmetric since early telescopic observations. It was observed frequently by TES during the MGS aerobraking phase as an offshoot of atmospheric monitoring for engineering purposes, during which the cryptic region was identified (Kieffer *et al*., 2000) as a dramatic discrepancy between the visual and thermal retreat. Continuing observations by TES, The Mars Odyssey Thermal Emission Imaging System (THEMIS), MOC, and OMEGA have shown that the asymmetric sequence repeats consistently.

The MOC observations of the global recession in 1999, 2001, and 2003 suggest that the overall seasonal cap is insensitive to global-scale dust storms. However, Bonev *et al*. (2005) showed evidence for local variations due to the redistribution of absorbed solar energy. During large dust storms, when the direct absorption of solar energy is reduced and thermal downwelling radiation is increased due to increased atmospheric opacity, bright regions of the cap have higher sublimation rates, while darker regions have lower sublimation rates. Inevitably, this means that the cryptic region lasts longer and features like the "Mountains of Mitchel" disappear earlier.

The southern seasonal cap has been observed by OMEGA from its maximum extent, close to the southern winter solstice, to the end of the retreat at L_s ~325°. It is spectrally dominated by CO_2 ice, consistent with previous temperature measurements by TES and THEMIS. During winter, the longitudinal distribution of CO_2 ice is relatively symmetric, in agreement with previous observations. H_2O ice, initially limited to regions close to the Hellas basin, extends eastward due to the sublimation–recondensation process initially proposed by Houben *et al*. (1997). The OMEGA observations are consistent with circulation models which demonstrate the major role of Hellas on weather patterns in the south (Colaprete *et al*., 2003; Montmessin *et al*., 2004). In early southern spring, the brightening of central regions of the seasonal cap is associated with a decrease in grain size and dust contamination. The development of a dark and cold region within the seasonal cap (the cryptic region) corresponds to extensive dust contamination at the surface of CO_2 ice (Langevin *et al*., 2006). At the time of maximum extent (L_s ~225°), the seasonal cap is very complex in terms of spectral signatures, with a few regions spectrally dominated by H_2O ice and a wide range of grain sizes and levels of dust contamination. From late southern spring to mid summer, most of the seasonal cap appears to be remarkably clean CO_2 ice with grain sizes ranging from a few millimeters to a few centimeters. During this season, H_2O ice appears to play very little role, either as frost on the surface or as icy aerosols (Langevin *et al*., 2007). The sublimation–recondensation process of H_2O ice, which is so effective in the north and in southern winter, is also not observed, most likely due to the very low amounts of available H_2O. Although the overall agreement with general circulation models is satisfactory (Montmessin *et al*., 2004; Langevin

et al., 2007), there are a few discrepancies (e.g., the extent of ice aerosols close to equinox, the lack of H_2O recondensation in late spring) that will help to further constrain climate models.

25.5.2 Seasonal cap mass and density

The mass of the polar caps is an important parameter in understanding the Martian climate. The distribution of seasonal CO_2 ice provides information about the interaction between the atmosphere, topography, and surface properties. The density of the CO_2 ice constrains several important polar processes, including deposition mechanisms and densification. Calculations and remote-sensing data that have been analyzed to determine seasonal cap characteristics are reviewed here, as is the use of neutron spectroscopy to determine CO_2 cap thickness.

Several approaches have been used to estimate the amount of CO_2 that condenses into the seasonal cap (see James *et al*. [1992] for earlier estimates). The most robust have been GCMs tuned to match the atmospheric pressure curves from the Viking landers (Tillman *et al*., 1993). While these models often use unrealistic albedo and emissivity for the seasonal caps, they do match the pressure curves, and therefore must match the net global accumulation; however, they do not necessarily match local distributions. Other methods use energy balance considerations. For example, Kieffer *et al*. (2000) computed the annual southern mass at several locations from thermal and albedo observations throughout the sublimation season, yielding 800 to 1200 kg m^{-2} (polar cap sublimation and accumulation budgets are often expressed in mass per unit area; e.g., for an assumed density of 1000 kg m^{-3}, a budget of 1200 kg m^{-2} would correspond to a thickness of 1.2 m). Kieffer and Titus (2001) used energy balance during both condensation and sublimation seasons in the north to estimate the zonal distribution of cap mass, not only finding peak budgets of $\sim$1100 kg m^{-2} near the pole, but also finding the condensation budget several hundred kg m^{-2} larger than the sublimation budget near 70° N, suggesting substantial zonal heat transport in the spring. This analysis, however, neglected the effects of heat storage in the regolith. The polar CO_2 condensation creates an observable increase in the planet's rotation rate by conservation of angular momentum (Folkner *et al*., 1997; Yoder and Standish, 1997). A combination of gravity and differential elevation measurements were used to estimate a seasonal cap density of 910 ± 230 kg m^{-3} (Smith *et al*., 2001a).

Nuclear spectroscopy measurements made by Mars Odyssey are sensitive to the column abundance (kg m^{-2}) of CO_2 surface ice, which has been monitored for over two Mars years. The GRS, NS, and High Energy Neutron Detector (HEND) instruments provide signatures that can be analyzed to map the distribution and mass of seasonal ice, with a spatial resolution of approximately 600 km (see Chapters 5 and 6). Signals from neutrons and gamma rays have different sensitivities to ice depth and are thus complementary. Gamma ray transmission measurements were used to map the column abundance of CO_2 ice in the northern and southern hemispheres (Kelly *et al*., 2006). The leakage flux of neutrons is sensitive to surface CO_2 ice because the ice does not strongly absorb neutrons and is a poor moderator in comparison to H. Therefore, neutron counting rates generally increase monotonically as ice is added to the surface (e.g., see Figure 25.6). Initial results were obtained from NS measurements, in which the data were analyzed to determine the column abundance poleward of 85° N. The column abundance was compared to GCM estimates of the mass (Feldman *et al*., 2003) and combined with MOLA thickness data to estimate density (Aharonson *et al*., 2004). The data were subsequently analyzed to determine the spatial distribution of ice in the north and south for two Mars years (Prettyman *et al*., 2005). The HEND data have also been analyzed to determine the local column abundance, mass, and density (in combination with MOLA data) of the seasonal caps in both hemispheres (e.g., Litvak *et al*., 2007). All of these techniques give results that are consistent with GCM predictions (tuned to Viking pressure data) of mass, to within the limits of their systematic and statistical errors. In addition, the mass and distribution of CO_2 were found to be consistent between the two years for which data have been acquired. The strength of the measurements is their ability to determine spatial distributions of CO_2, which can be used to further understand polar circulation and dynamics, as well as to constrain the polar energy balance and to improve physical models of condensation and cap properties for GCMs.

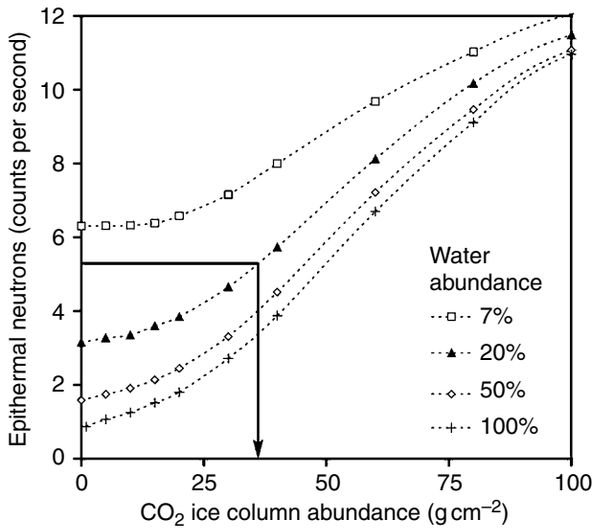

Figure 25.6. Epithermal neutron counting rate as a function of CO_2 ice column abundance. The CO_2 ice covers four different homogenous regolith materials, consisting of soil mixed with water ice. The abundance of water ice for each material is indicated in the legend. If the abundance and stratigraphy of water equivalent hydrogen is known, then the column abundance of CO_2 ice can be uniquely determined, as indicated by the arrow.

To illustrate the information provided by nuclear spectroscopy, counting rates measured by the NS poleward of 60° show a strong seasonal variation (Figure 25.7). Counting rates for three distinct energy ranges measured by the spectrometer (fast, epithermal, and thermal) are shown. The observed variations are caused primarily by changes in the

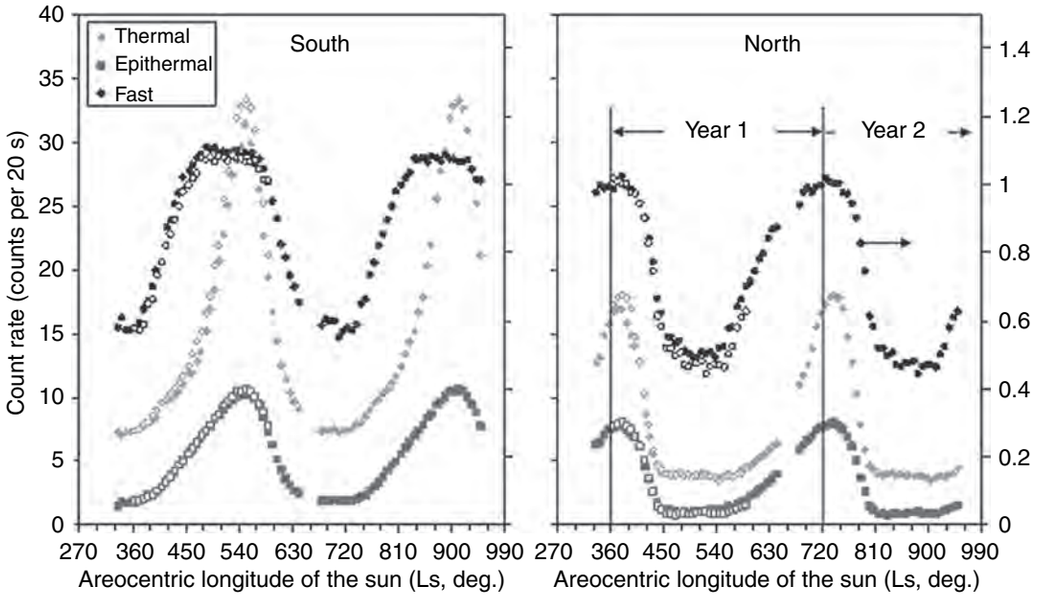

Figure 25.7. Time series Mars Odyssey NS instrument neutron counting data binned poleward of 85° S (left) and 85° N (right) from February 2002 to July 2005. Time is given in terms of the areocentric longitude of the Sun (L_S), or season. Each point is averaged over roughly 7° of L_S. $L_S = 0°, 360°, 720°, \ldots$ corresponds to the vernal equinox in the northern hemisphere. $L_S = 90°, 450°, 810°, \ldots$ corresponds to the northern summer solstice. Successive years are arbitrarily labeled "Year 1" and "Year 2." Data from the second year (shown as open symbols) were shifted and superimposed on the first year to show the level of inter-annual variations.

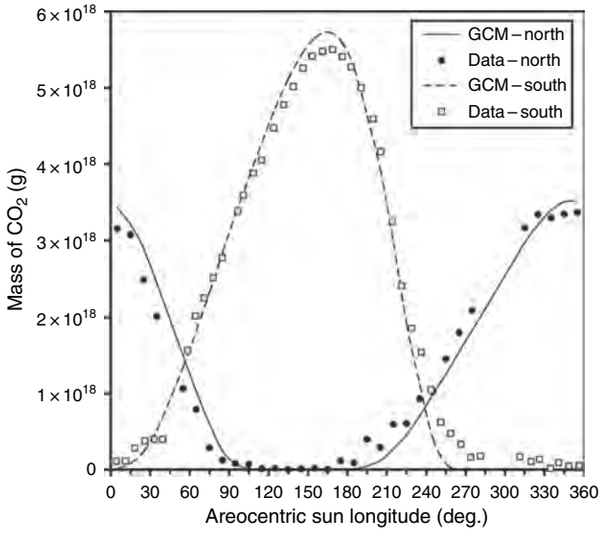

Figure 25.8. The total mass of seasonal CO_2 ice poleward of 60° is shown for the northern and southern hemispheres, determined from epithermal neutron counting data (points) and estimated by a GCM calculation (lines). In the GCM calculation, the seasonal cap albedo and emissivity were adjusted to match the seasonal pressure variation observed at the Viking landing sites. (The GCM results are courtesy of NASA Ames Research Center and the New Mexico State University Department of Astronomy.)

polar surface and atmosphere as CO_2 ice condenses onto and sublimes from the surface. For all three energy ranges, the counting rate begins to increase in the fall during the polar night as CO_2 ice forms on the surface, achieving a maximum in the winter, and decreasing again during spring as the CO_2 sublimes. Each energy range has a unique time profile, which reflects their different sensitivities to CO_2 ice. Generally, the counting rates do not vary between Years 1 and 2, which implies that the polar inventory of CO_2 ice does not vary significantly from year to year. The counting rates are converted into CO_2 ice column abundance using the relationships shown in Figure 25.6, which were determined by modeling cosmic ray interactions with the Martian surface and atmosphere.

The total mass of seasonal CO_2 ice poleward of 60° was determined for Year 1 from the epithermal counting data for the northern and southern hemispheres and is compared to a GCM calculation in Figure 25.8. For the GCM calculation, the emissivity and albedo of the seasonal frost, which were assumed to be uniform, were adjusted so that the results of the calculation matched the seasonal pressure variation measured by the Viking landers in the 1970s (Hourdin *et al.*, 1995; Haberle *et al.*, 1999). Differences between the GCM calculations and the GRS/NS/HEND estimates are relatively small, which suggests that the seasonal cap evolution has not varied significantly over thirty years. Estimates of the total cap mass varied between 3 to 4×10^{15} kg for the northern cap and 3 to 6×10^{15} kg for the southern seasonal cap. Local variations in CO_2 column abundance are shown in Figure 25.9 for the northern and southern hemispheres.

Measurements of density are more reliable than measurements of mass, probably owing to uncertainties in linear thickness measurements and comparisons between regionally averaged frost values (from nuclear spectroscopy) and local measurements provided by MOLA. Density estimates for the northern seasonal cap vary from 500 to 1100 kg m^{-3} (e.g., Smith *et al.*, 2001a; Aharonson *et al.*, 2004; Smith and

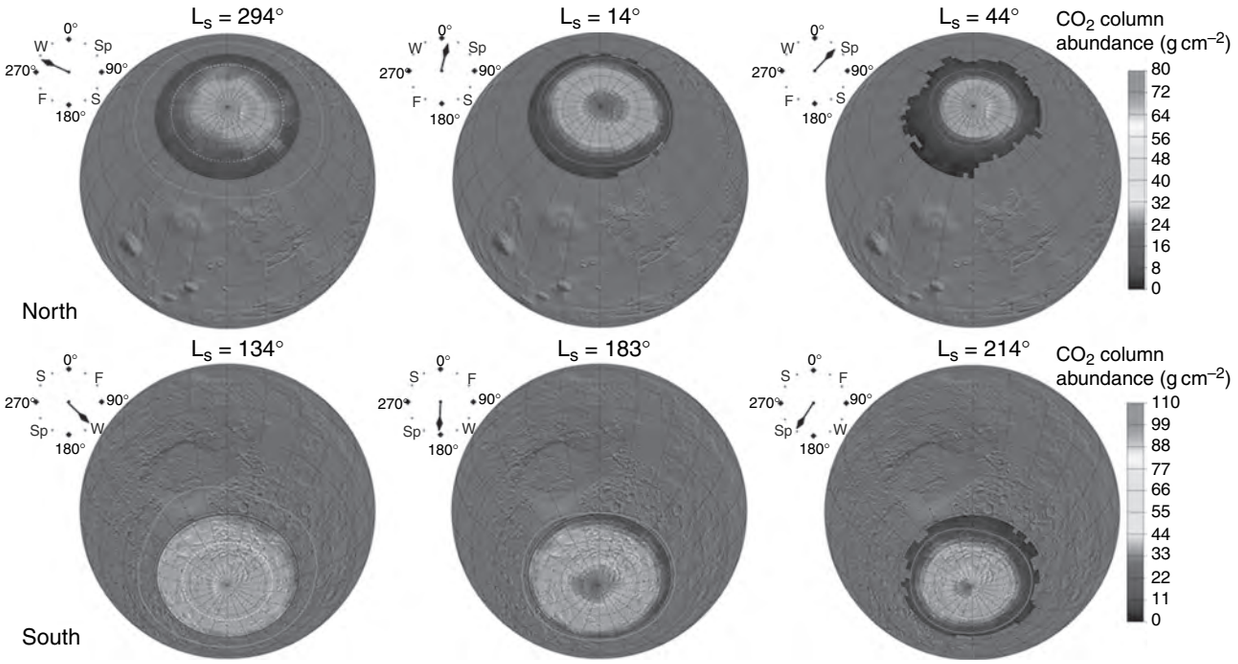

Figure 25.9. Maps of CO_2 column abundance in the northern and southern hemispheres (poleward of 60°) are compared to cap edge functions (solid red line) and the extent of the polar night (dashed green line). In both hemispheres, the maximum column abundance occurs near the pole during the recession. In the southern hemisphere, the distribution is asymmetric, with peak column abundance occurring at the location of the perennial CO_2 cap. (For a color version of this figure, please refer to the color plate section or to the online e-Book version of this chapter.)

Zuber, 2005) depending on how the estimate was determined and over which latitude region. The southern seasonal cap appears to have a density of ~1000 kg m^{-3}. The density of the seasonal cap may not be constant, but may vary over latitude and season. The density can vary due to the mechanism of deposition (e.g., direct condensation versus snowfall). The density of the CO_2 ice can also change over time due to densification. Impurities, such as dust or H_2O, can also affect density. Finally, the presence of noble gases can create bubbles inside the CO_2 ice, thus increasing its porosity.

25.5.3 The cryptic region

The cryptic (meaning obscure or camouflaged) region, a dark and cold region within the southern seasonal cap, has been identified as "dark and dirty" dry ice (Titus *et al*., 1998, Kieffer *et al*., 2000). While these authors were the first to recognize the cryptic region as dark CO_2 ice, they were not the first to have observed the region. Observations of this dark seasonal feature date back to 1845, when first seen by the American astronomer Ormsby MacKnight Mitchel (Blunck, 1982).

AQ3

This southern springtime phenomenon was also observed by several astronomers through the late nineteenth and early twentieth centuries. In 1892, Barnard, Hussey, Schaeberle, and Young observed the cryptic region from L_s ~210° to 229°. The cryptic region was again observed in 1894 by Barnard, Pickering, and Lowell (L_s ~ 206°–237°). Fournier observed and drew an illustration (L_s ~235°) of the cryptic region in 1909. In 1924, Antoniadi (1930) observed this region, which he called *Depressio Magna* (~80° S, 270° W), or Big Depression. Antoniadi even speculated that this dark region inside the bright seasonal cap might be a polar lake. In addition to the observation of *Depressio Magna*, Antoniadi also observed a smaller dark patch, which he referred to as *Depressio Parva* (Little Depression). These two dark patches correlate with the location of the cryptic region as observed by both the Viking Orbiter Infrared Thermal Mapper (IRTM) and MGS TES. *Depressio Magna*, or what is presently referred to as the cryptic region, can still be seen in the best ground-based images taken of Mars around favorable oppositions.

The two Viking Orbiter IRTM instruments were the first thermal IR instruments to observe the southern retreating cap (Kieffer, 1979). While observed by the IRTM (Figure 25.10a), the cryptic region was not fully recognized as a region of dark CO_2 ice and was relegated to a footnote in a paper by Kieffer (1979).

With the arrival of MGS, three new instruments were observing the cryptic phenomenon: a high resolution optical camera (MOC), a thermal IR spectrometer (TES, a thermal spectrometer and bolometer and a solar bolometer with ~3 × 6 km resolution), and MOLA, which, when operated as a reflectometer, could map the cap albedo at a wavelength near 1 μm.

The TES bolometers revealed a region of the springtime southern cap that was cold and dark (Figure 25.10b). Spectra from TES did not show the 25 μm transparency band, typical of fine-grained CO_2 frost and snow, suggesting that the cryptic region was composed of either coarse-grained

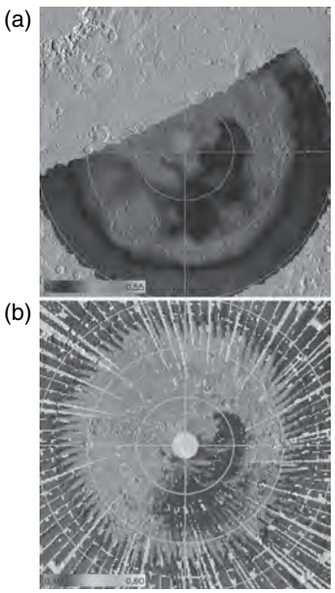

Figure 25.10. Albedo of the cryptic region. (a) The albedo of the southern seasonal cap in 1976 as measured by the Viking IRTM solar channel bolometer. (b) The albedo of the southern seasonal cap in 1999 as measured by the MGS TES solar channel bolometer. (For a color version of this figure, please refer to the color plate section or to the online e-Book version of this chapter.)

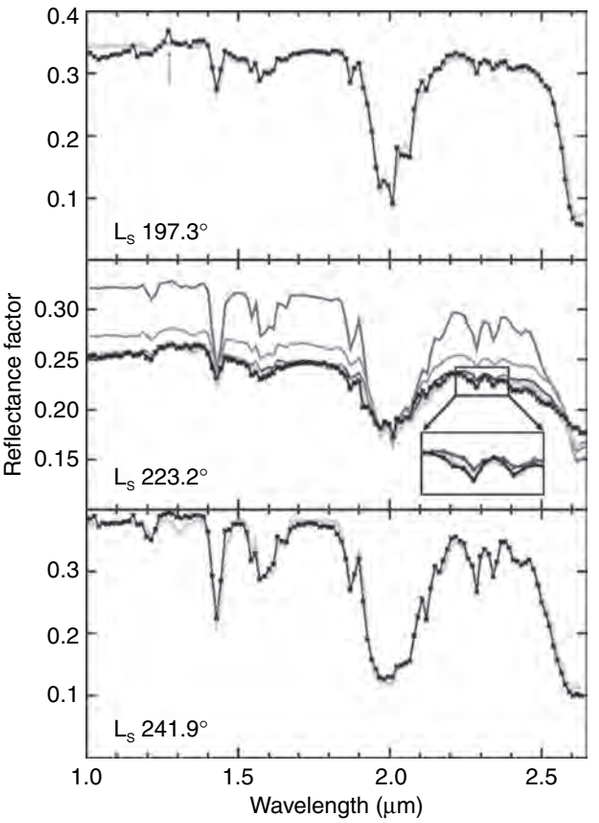

Figure 25.11. The black lines correspond to observed OMEGA reflectance spectra of the cryptic region (82° E, 85° S) at three values of L_s (197.3°, 223.2°, 241.9°). The thick green lines correspond to best fit model spectra, including dust, water ice, and CO_2. In the middle panel ($L_s = 223.2°$), the sensitivity of the models to different parameters is examined, in particular to the dust contamination within surface layers (red: 50% less dust) and the thickness of the CO_2 layer (blue curve in the insert: 7.5 cm instead of 15 cm; Langevin *et al*., 2006). (For a color version of this figure, please refer to the color plate section or to the online e-Book version of this chapter.)

or slab CO_2, or dirty dry ice. While thermal IR spectral observations could not determine the form of CO_2 ice that composed the cryptic region, other observations provided indirect evidence that supported the concept of a coarse-grained translucent slab. For example, MOC images, with resolution as high as ~1.5 m/pixel, revealed that the cryptic region had a cornucopia of bizarre albedo features that have been referred to as a "zoo" (Kieffer *et al*., 2000, 2006; Kieffer, 2007). Subkilometer dark areas were observed within the seasonal frost. Also discovered were fields of dark, round spots with parallel-oriented tails ("fans"), fields of spots with individual or collective medium-toned halos, and fields of dark (later to become relatively light) radial and ragged branching patterns ("black spiders"), usually centered on the narrow ends of fans (Piqueux *et al*., 2003). Some of the spots must form in the dark, as they are observed in prepolar-drawn images (Aharonson *et al*., 2004).

The initial interpretations, based solely on imaging, of these dark surfaces within the polar frost were that they were defrosted surfaces and should be warm (Malin *et al*., 1998). However, the TES instrument observed low temperatures in the cryptic region for weeks and months after the formation of the spots and fans, indicating that solid CO_2 was still present at the surface. A small diurnal temperature variation (~5 K) suggested the possible presence of either a thin layer of surface dust or a layer of near-surface atmospheric dust (Kieffer *et al*., 2000; Titus and Kieffer, 2001). The THEMIS simultaneous visual and thermal imaging of these features with 100 m resolution or better confirmed the TES inference that they were entirely at solid CO_2 temperatures for much of the spring. Once the spots begin to warm, however, they grow and coalesce quickly, forming large defrosted regions (Kieffer *et al*., 2006). All the albedo features disappear when the ground warms, except the "spiders," which are observed as depressions when the cap is gone.

With the arrival of Mars Express, NIR and short wave mid-IR hyperspectral imaging observations became available. The OMEGA spectrometer has provided additional information about the cryptic region through the analysis of H_2O and CO_2 ice absorption features. Spectral modeling has proven very successful for the interpretation of OMEGA observations. As an example (Figure 25.11), the evolution of the observed spectrum from the cryptic region during the southern spring (L_s ~197°) can be interpreted first as an intimate mixture of dust (0.7 wt.%) and H_2O ice (0.06 wt.%) within CO_2 ice. Later (L_s ~223°), there is evidence for extensive contamination of the surface layers by ~7 wt.% of dust. Finally, two weeks before the area becomes completely free of ices (L_s ~242°), the spectra are consistent with areal mixing of 25% ice-free areas and 75% ice-covered areas within each pixel. Such subkilometer-scale ice-free and ice-covered areas are a consistent feature of regions close to

the sublimation front at all stages of the retreat of the southern seasonal cap.

Hypotheses

A series of unanticipated observations by the MGS TES and MOC, with confirmation by THEMIS (Kieffer *et al.*, 2006), has led to a complex model for surfaces processes in the seasonal polar cap. All of the cryptic region features described above were observed by THEMIS to occur at solid CO_2 temperatures and to stay that cold for weeks to months. A possible explanation pivots on the physical and optical properties of solid CO_2, which has a very small absorption coefficient in the solar wavelength region and becomes opaque to thermal radiation within a few millimeters thickness (Hansen, 1997, 2005; Kieffer, 2007). H_2O and dust are also involved in this proposed explanation that is summarized by a brief description of the annual sequence based on the discussion by Kieffer (2007).

Deep in the Martian polar night, there is some CO_2 snowfall, but most of the solid CO_2 takes the form of a uniform, continuous, nonscattering slab with embedded dust (and H_2O ice) grains. Predawn seasonal heat flow sublimes CO_2 and some "vents" form to release this gas. Following seasonal sunrise, in some areas the ice brightens due to fracture or surficial frosting, but in other areas the slab persists to form the dark, cold cryptic region. Here, the solar energy is largely absorbed by embedded dust grains (which either burrow downward or escape upward), cleaning the CO_2 slab and annealing small holes near its surface. Sunlight then penetrates to the bottom of the slab, warming the soil and subliming ice from the bottom. Some unidentified process causes a slight uniform darkening of the slab around vents to form "halos." The CO_2 at the bottom of the slab sublimes and forces gas into the subsurface. Additional vents develop that allow this gas to escape. As the sub-slab gas converges toward the vents, it scours the soil surface along ragged channels (spiders). Dust entrained in the jetting gas falls out downwind to form "fans." As the slab thins and the sub-slab pressure drops, gas enriched in water vapor is released from the subsurface to cool and deposit water frost in the channels, brightening the spiders. As soon as the CO_2 slab is gone, the water frost warms and evaporates. Only the topographic ghosts of the spiders persist through the summer. Thus, seasonal reworking of the soil below the ice slab may help to explain the uniformity and youthful appearance of the terrain upon which the vents form.

This venting model is mainly based on visible and thermal IR observations. The results of OMEGA spectroscopy presented by Langevin *et al.* (2006) raised major questions, however, as most of the cryptic region in mid spring ($L_s \sim 220^\circ$) did not exhibit the spectral signature of a clear slab of CO_2 ice, which is the most favorable configuration for the venting model. Instead, the surface of the CO_2 ice appeared strongly contaminated by dust, with few photons making it to the underlying surface. These observations led to a hypothesis in which dust could be deposited on the surface shortly after equinox by storm systems originating from the Hellas region (Colaprete *et al.*, 2005). Additional surface dust could be provided by dust initially embedded with the CO_2 ice slab. Dust trapped within the ice would warm under sunlight, subliming the ice and allowing the dust particles to escape. The largest dust grains would burrow down to the surface underlying the ice, while the smallest dust grains would blow away with the sublimation winds (Kieffer, 2007).

These hypotheses are not mutually exclusive. The venting model is the best candidate to explain the spots, fans, and spiders observed at different times and places in the seasonal cap. However, heavy contamination by surficial dust (either due to venting or due to other dust sources) markedly decreases the proportion of solar photons reaching the underlying surface, thereby reducing the efficiency of the venting process. One of the possibilities to be considered is that the venting process is mainly active very soon after sunrise at high southern latitudes, close to equinox. Another source of dust may play a role either simultaneously with venting or at a later stage, as large areas in the cryptic region do not exhibit features such as spiders, spots, and fans that would indicate that the venting process had been active. New high resolution observations by CRISM and HiRISE (HiRISE – High Resolution Imaging Science Experiment), new observations and modeling from OMEGA, and more laboratory work will all be needed to improve our understanding of the wide diversity of processes at work at high southern latitudes.

Cryptic region location

Why is the cryptic region located where it is on the seasonal cap? Initial attempts to find correlations of the cryptic region's location with local geologic features failed (Kieffer *et al.*, 2000). A majority of the cryptic region lies over the PLDs, but it also extends over other geologic units. Intraseasonal and interannual variations in the shape of the cryptic region suggested that atmospheric dynamics might play a role. Indeed, this hypothesis has gained additional support from mesoscale modeling that has demonstrated that regional topography (primarily the Hellas basin), sets up an $N = 1$ standing wave during the southern winter (Colaprete *et al.*, 2005). The standing wave appears to cause two distinct microclimates to form over the southern polar region: the western hemisphere (longitudes 210° E–30° E, south and southwest of Argyre) is colder, cloudier, and has more snowfall, while the eastern hemisphere (longitudes 30° E–210° E, south and southeast of Hellas) is slightly warmer and wetter (higher water-vapor abundance). The cryptic region lies in the "warmer and wetter" microclimate, where there is less snowfall and enhanced radiative loss to space.

25.6 PERMANENT DEPOSITS

25.6.1 Residual caps

Viking observations of large increases of atmospheric water after seasonal cap sublimation (Farmer *et al.*, 1976) and

temperatures well above those possible for CO_2 ice (Kieffer *et al*., 1976) led to the conclusion that the north residual cap is water ice, while the persistently low temperature of the south residual cap (Kieffer, 1979) showed that to be CO_2. This was a surprising conclusion of disparate surface compositions! However, during one season (in 1969), enhanced atmospheric water observations over the South Pole suggested that a CO_2 cover over the south cap may have sublimed (Jakosky and Haberle, 1990).

Thus, the Viking era view of the Mars residual caps was one with a large H_2O ice cap in the north and a smaller CO_2 cap in the south. Since the arrival of MGS, however, this view has changed. Specifically, now the South Polar residual cap (SPRC) is also believed to be an H_2O ice cap, but with a decameter-scale veneer of CO_2 ice that remains through most southern summers.

Observations in the era between Viking and MGS are summarized in Chapter 2 of this book. More recent observations by Thomas *et al*. (2000) using MOC imagery show that the north cap grades into the underlying layered materials while the south cap appears as a distinct geologic unit with very different topography than the surrounding layered terrains. Observations by MOLA (Zuber *et al*., 1998; Smith *et al*., 2001b) provided estimates of total residual cap plus polar layered deposits volumes but did not constrain relative proportions of dust and ice within the caps.

Dark and layered markings in the interior of the residual caps were noted in Mariner 9 observations and subsequently mapped in detail with Viking (e.g., Cutts and Smith, 1973; Soderblom *et al*., 1973; Cutts *et al*., 1976; Tanaka and Scott, 1987; Thomas *et al*., 1992). These features include troughs, scarp faces, and the large and broad re-entrant valleys Chasma Boreale and Chasma Australe. Exposures in these regions are finely layered and generally much darker than the surrounding ice surfaces. Zuber *et al*. (1998) showed that the troughs and chasmata are quite deep, cutting up to 1 km into the ice surface. Models for formation and migration have variously included accumulation, wind ablation, glacial flow, and sublimation; the history and arguments for all these processes have been recently summarized by Howard (2000), Ivanov and Muhleman (2000), and Fisher (2000). The study by Durham *et al*. (1997) on ice rheology revived the glacial flow hypothesis; however, current deformation rates from glacial flow may be minimal at present polar temperatures. Even if the trough surfaces migrate poleward, timescales for migration remain uncertain. It is generally presumed that the layers exposed in the troughs provide a record of cap evolution or climate history. In the north, the layered deposits cover nearly the same area as the residual cap, while in the south the layered terrains are much more extensive than the permanent ice deposit (e.g., Thomas *et al*., 1992). Among geologists, the layered terrains are often discussed as including the overlying permanent ice as part of the unit. Paige *et al*. (1994) found that both the permanent ice cap and the layered deposits in the north had very high thermal inertias, which they interpreted as indicating coarse-grained or solid water ice for at least 1 m under the residual cap and also underlying the layered deposits. In contrast, the South PLDs show a systematic poleward decrease in thermal inertia, interpreted as aeolian deposits, while the south residual cap again had very high thermal inertia (Paige and Keegan, 1994). Zuber *et al*. (1998) suggested that polar outliers in the north are likely soil-covered ground ice and that the north permanent cap was previously larger in spatial extent.

North Polar residual cap

Examination of the northern residual ice cap showed a change in albedo in a number of North Polar bright ice outliers and in the overall coverage by bright ice deposits between Viking and Mariner 9 and between Viking Orbiter summers (Kieffer, 1990; Paige *et al*., 1994; Bass *et al*., 2000). These changes were attributed to the possible effects of global dust storms (Paige *et al*., 1994); however, Bass *et al*. (2000) showed that significant variations occurred within the summer season among Viking images. Cantor *et al*. (2002) also examined such variations in MOC images and noted brightening at the cap edges within a given Mars summer season as well as changes in the cap appearance at the same L_s (areocentric longitude) between the first two MGS years. The early season appearance was possibly attributed to the occurrence of a large dust storm the previous year, and it was noted that late season ice extent recovers to Viking levels but exhibits small-scale inter-year variations that may not be related to globally repeated weather events.

The evolution of the north perennial cap was monitored with OMEGA in late 2004 (Langevin *et al*., 2005). These observations confirmed that the north perennial cap consisted of H_2O ice. Imaging spectroscopy in the NIR range provides strong constraints on ice grain sizes. The OMEGA observations demonstrated that the albedo of the ice-covered regions is controlled by a combination of all the parameters which had been considered as potentially contributing to albedo changes by Kieffer and Titus (2001): (1) Seasonal frost, with grain sizes $<100\,\mu m$, is brighter than permanent ice, with grain sizes up to 1 mm in mid summer; (2) Dust contamination in surface layers lowers the albedo; and (3) When the optical thickness of aerosols is large, albedo contrasts decrease because the apparent albedo of bright ice-covered regions decreases while that of the dark surrounding regions increases.

In the central part of the cap, the decrease in albedo observed during early summer ($L_s = 93^\circ$–110°) is a result of the sublimation of fine-grained seasonal frost, exposing coarser-grained permanent ice underneath. Patches a few tens of kilometers in extent at the edge of the permanent cap remain bright throughout summer, most likely corresponding to accumulations of small ice grains. In the outlying regions, defrosting occurs before solstice, and the albedo and band strengths increase in early summer due to a combination of a decrease in surface dust contamination and a decrease in aerosol opacity in early summer.

Calvin and Titus (2007) used TES observations from three Martian years to monitor large-scale variations in the north residual ice cap (Figure 25.12). These observations monitor the defrosting process during spring and early summer, confirming that the central parts of the cap undergo a period of

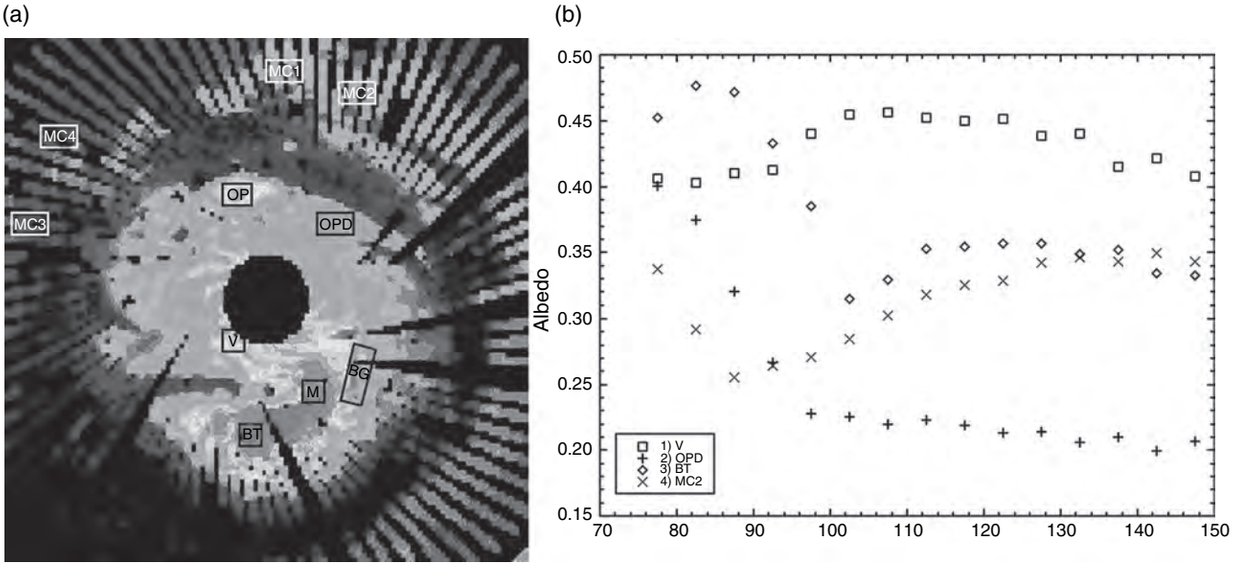

Figure 25.12. (a) Regions identified using TES albedo channels where frost mobility over the summer was noted. Color scale is TES albedo at $L_s = 85$ from 0.15 to 0.5 (purple to red). (b) Seasonal trends in albedo for the four types described in the text. (For a color version of this figure, please refer to the color plate section or to the online e-Book version of this chapter.)

defrosting up to L_s ~100° to 105° as temperatures warm. Then, as temperatures begin to cool, higher elevations cold-trap new frost. Outlier ice deposits also preferentially cold-trap frosts later in the summer, although coarse-grained ice continues to dominate the ice spectra. Processes involved in frost mobility are as varied as the terrains in the North Polar Region, but albedo, temperature, and elevation appear to exert the strongest controls. While large scale patterns remain the same, there is some amount of interannual variability in both the persistence and location of the highest albedo deposits. Over the course of the summer season, four major trends were observed: (1) Two odd patches stayed bright throughout the summer; (2) Peripheral areas defrosted to nonice material and stayed thereafter at a low albedo; (3) Cap materials defrosted to icy material that is coarser or dirtier than early spring ice; and (4) Outlier deposits defrosted early but then re-accumulated bright frost late in the summer season. The location and persistence of cold and bright patches may depend on heterogenous deposition in the previous winter, or on the locations of cold spots influenced by winds or precipitation during the polar night (e.g., Titus *et al.*, 2001).

South Polar residual cap

The disaggregated appearance of the SPRC and a single ground-based observation of unusually high water-vapor abundance in the southern hemisphere (Barker *et al.*, 1970) lead many to speculate that the southern CO_2 ice residual cap might only be a "thin" veneer covering an H_2O cap, and that in some years the CO_2 ice completely sublimes, exposing the underlying H_2O ice (Jakosky and Haberle, 1990).

While the complete disappearance of the CO_2 ice veneer has never been directly observed, there are several observations indicating that the SPRC is mainly H_2O ice. The flood of evidence started with MGS observations and continues with Mars Express observations. One of the clues from the post-Viking era was topographical modeling conducted by Nye *et al.* (2000) with MOLA elevation data. They showed that the SPRC could not retain its current shape if it was composed of CO_2, but would be stable if composed of dirty H_2O ice. Warm temperatures (<200 K) were observed by THEMIS in the interior of the cap (Byrne and Ingersoll, 2003) and around the edge of the cap (Titus *et al.*, 2003). The MGS TES confirmed that the thermal inertia of the warm temperature regions at the edge of the SPRC was consistent with high thermal inertia material, presumably H_2O ice. Neutron spectroscopy data from the Mars Odyssey GRS/NS/HEND are consistent with an H_2O cap covered by CO_2 ice.

The south perennial cap was first observed by OMEGA at a relatively low resolution (3 km) in January 2004, shortly after the orbit insertion of Mars Express, then at a higher resolution (300 to 500 m) in early 2006. These observations revealed a widespread contamination of the dominant CO_2 ice component by H_2O ice and dust, and patches of H_2O ice heavily contaminated by dust have been observed around the perennial cap (Bibring *et al.*, 2004; Douté *et al.*, 2007).

Swiss cheese and CO_2 veneer thickness

With the advent of high resolution imaging of the SPRC came the discovery of a new terrain type, dubbed "Swiss cheese" terrain (Figure 25.13; Thomas *et al.*, 2000) because it consists of a network of swirl-covered mesas and circular pits that cover much of the SPRC. Both thermal and NIR imaging has shown that many of these pits reach to an underlying H_2O ice unit (Byrne and Ingersoll, 2003; Bibring *et al.*, 2004), presumably an H_2O ice cap similar to, but smaller than, the north polar residual cap (NPRC). Early measurements (Malin *et al.*, 2001) concluded that some scarps were retreating at ~2 m/Mars year. A more

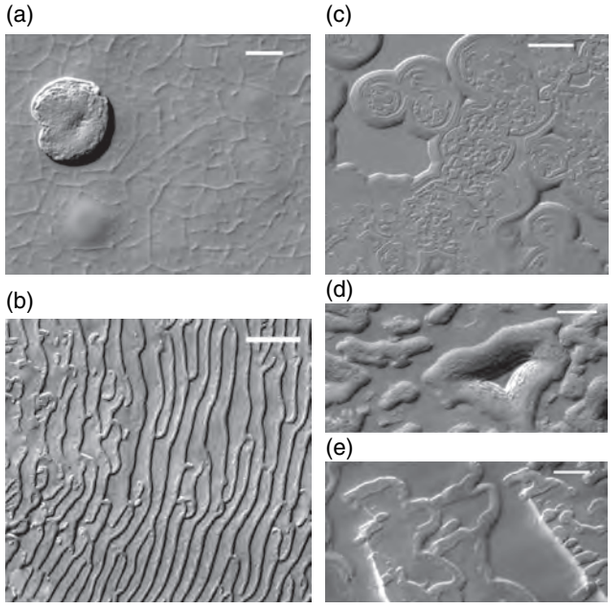

Figure 25.13. Examples of South Polar residual cap "Swiss cheese" topography. (a) Nearly circular depression and polygonally cracked sag surface on top layer. Portion of MOC image M09-000609; 87.0° S, 5.9° W, acquired at $L_s = 237.3°$; Scale bar is 100 m and illumination is from the lower right. (b) "Fingerprint" pattern of depressions. Portion of MOC image M03-06756; 86.0°S, 53.9°W, acquired at $L_s = 182.4°$; Scale bar is 500 m and illumination is from lower right. (c) Circular collapse features, leaving mesas on upper surface with debris aprons and moats. Largest scarps here are about 4 m high. Portion of MOC image M03-06646; 85.6° S, 74.4° W, acquired at $L_s = 181.3°$; Scale bar is 500 m and illumination is from lower right. (d) Residual mesa exposing four layers and surrounding moat. Portion of MOC image M07-02129; 86.9° S, 78.5° W, acquired at $L_s = 204°$; Scale bar is 100 m and illumination is from bottom right. (e) Complex covering of depressions which suggest burial and exhumation of topography on part of the southern residual cap area. Portion of MOC image M04-03877; 84.6° S, 45.1° W, acquired at $L_s = 196°$; Scale bar is 200 m and illumination is from the lower right. (Figure from Thomas *et al*., 2000.)

detailed study by Thomas *et al*. (2005) concluded that there were two types of Swiss cheese, an older thicker unit and a younger thinner unit. The older unit, which is typically less than 15 m thick and composed of several layers ~2 m thick, is backwasting at a rate of ~3.6 m/Mars year. The younger unit, which is composed of 1 to 3 layers, each ~1 m thick, is backwasting at a rate of ~2.2 m/Mars year. Other studies (e.g., Titus *et al*., 2003; Winfree and Titus, 2006), have suggested that the residual cap may actually be getting larger in at least a few locations and that the circumpolar exposed water ice and outliers may mark the location of the SPRC in the not-to-distant geologic past.

The rheology of solid CO_2 at temperatures slightly higher (150 to 190 K) than the Martian polar caps was measured by Durham *et al*. (1999); deformation followed $\varepsilon' = A\ \sigma e^{Q/RT}$ where R is the gas constant, A is $10^{3.86}$ MPa^{-n} s^{-1}, $n = 5.6$, and $Q = 33$ kJ mol^{-1}. This is much weaker than solid H_2O; the regional profiles and probable age of the perennial south cap are thus not compatible with a bulk composition of CO_2. High resolution imaging suggests that the perennial CO_2 is only a few meters thick; the underlying material is probably ice-saturated PLDs.

How thick is this "thin" veneer of CO_2 ice? What percentage of the H_2O ice is covered and how much is exposed? Tokar *et al*. (2002) and Prettyman *et al*. (2004) tried constraining the answers by using variations in the neutron flux as Mars Odyssey flew over the SPRC. They were able to constrain the answers between two endmembers: a cap completely covered by a uniform veneer of CO_2 ice 160 g cm^{-2} thick, or a cap partially covered by thick CO_2 ice (greater than 1000 g cm^{-2}). If one assumes a density of 1 g cm^{-2}, then the column density estimates from their analysis are equivalent to either a cap completely covered by a veneer 1.6 m thick or a partially covered water-ice cap where the CO_2 cover is at least 10 m thick over 45% of the cap. Analyses of Swiss cheese terrain within the cap interior (Byrne and Ingersoll, 2003; Thomas *et al*., 2005) suggest that the CO_2 cover is between 8 and 11 m thick, more consistent with the thick partial coverage endmember. However, thermal observations during the mid summer would suggest a cap with a lower percentage of exposed ice, thus supporting the thin uniform layer endmember. The actual thickness of the CO_2 veneer is an important parameter in determining the current stability of the CO_2 SPRC (Jakosky and Haberle, 1990).

The offset of the SPRC from the geographical pole has been an outstanding mystery. But recent studies (Colaprete *et al*., 2005) suggest that the same atmospheric dynamics that may cause the deposition of dry ice that remains dark throughout the spring (the cryptic region, see Section "Cryptic region location") may also preferentially deposit snow at the present location of the SPRC.

25.6.2 North Polar erg

Surrounding the North PLDs is a vast unit of dark dunes sometimes called a "sand sea" or "erg" (Tsoar *et al*., 1979). The dunes are inferred to form, at least in part, from material eroded from the layered deposits, and volume estimates support this view (e.g., Lancaster and Greeley, 1990). In contrast to the layered deposits, however, the dunes were found to have very low thermal inertias (Paige *et al*., 1994) and their inertias are much lower than dark dunes elsewhere on the planet (Herkenhoff and Vasavada, 1999). Bell *et al*. (1997) noted that the dunes also have a different short-wave NIR spectral signature in images from the Hubble Space Telescope. The dunes appear to have a surface coating of gypsum as identified by OMEGA (Langevin *et al*., 2005). The gypsum deposits appear to have the largest concentrations near the mouth of Chasma Boreale, decreasing toward the west. Recent CRISM observations imply that the gypsum is concentrated along the dune crests rather than in the troughs (Roach *et al*., 2007). Both CRISM and OMEGA observations suggest that the basal unit of the PLD is not the source of the gypsum. However, CRISM has identified small outcrops of bedrock that do contain gypsum (Roach *et al*., 2007), and thus the bedrock is a possible source.

25.7 CURRENT STATE OF KNOWLEDGE

25.7.1 How far have we come?

At the end of Chapter 27 of the 1992 University of Arizona Press book *Mars*, James *et al.* (1992) presented several outstanding questions regarding Martian polar cycles and studies. In light of recent discoveries since then, here we consider how much our understanding has advanced, but also what old problems remain and new enigmas have emerged.

Suppression of winter condensation Comparisons of Viking pressure curves to energy budget considerations suggested that the condensation of CO_2 was being suppressed either by cloud effects or low emissivity. The recent discovery of near-surface H_2O ice in the high latitudes suggests that autumnal sublimation occurs, thus reducing the net accumulation of CO_2 ice throughout the fall and into the winter. Fall and early winter upward flow of heat from the regolith has now been modeled to have a significant effect, especially at latitudes where water ice is near the surface.

Significant spatial inhomogeneity of the seasonal caps Lateral differences in the surface properties of the CO_2 ice certainly play a role. The driving force may be standing waves in the atmosphere set up by the large southern basins.

Differences in the spring regression curves Seasonal pressure curves which are similar from year to year even with vastly different climate conditions have perplexed modelers. Recent analyses suggest that interannual weather (e.g., large-scale dust storms) affects the sublimation rate of the seasonal cap, but in such a way that local effects cancel out on the global scale.

Different natures of the residual caps The two residual polar caps are not as different as was believed in 1992. Both caps are water-ice caps. The southern cap retains a thin veneer of CO_2 ice throughout most summers. The other major difference that remains is that of the size of the caps, with the northern cap significantly larger.

The offset of the SPRC from the pole The driving force may be low-order standing waves in the atmosphere, set up by the large southern basins.

The stability of the residual CO_2 The stability of the SPRC remains an outstanding mystery. Several studies have suggested that the SPRC is thinning in the Swiss cheese regions. Other studies have suggested that the cap may be growing in places. With the arrival of Mars Reconnaissance Orbiter and its high-resolution VIS and NIR cameras and spectrometer, a dedicated polar monitoring campaign is underway to try to address this question.

25.7.2 Unresolved issues

There are as many unresolved issues in Martian polar science as ever, and new data seem to only deepen certain enigmas. Outstanding questions include:

- What is the nature of the CO_2 ice deposits ("Swiss Cheese," "slab ice," "cryptic regions," etc.), and the detailed processes responsible for their evolution?
- What are the seasonal and longer timescale variations in water-ice properties (e.g., grain size, compaction, accumulation, and loss zones in the northern residual cap)?
- What is the composition and amount of nonice material in the residual caps?
- How much water ice underlies the southern residual cap, and how often is it exposed?
- What is the relationship of dark materials in the windswept lanes and re-entrant valleys of the polar caps to the surrounding dark dune and surface materials?
- What is the relationship of the ice deposits to the underlying layered units, and why do they differ from the north to the south?
- What is the nature of seasonal and longer timescale obliquity variations, and what are their connections to the fine laminations of the PLDs?

ACKNOWLEDGMENTS

We acknowledge the extremely useful comments of Gary Hansen, Larry Soderblom, Kenneth Herkenhoff, and Jim Bell in the review of this chapter.

APPENDIX: INFORMATION ON PHYSICAL PROPERTIES OF MARTIAN ICES

H_2O ice

Physical property values for water ice are widely available, although commonly under terrestrial conditions; compilations can be found in the treatise by Hobbs (1974) and on the web at http://www.lsbu.ac.uk/water/data.html and http://skua.gps.caltech.edu/hermann/ice.table2.html.

CO_2

Physical property values for CO_2 are dispersed throughout the literature and are largely oriented toward commercial use. No compilation appropriate for Mars beyond that in James *et al.* (1992) has been assembled. Some additional information and values are summarized here.

There have been no recent measurements of the CO_2 saturation relation; the Clausius–Clapeyron relation is within 1% in pressure and 0.1 K in temperature of observations over Martian polar conditions (120 to 160 K) (James *et al.*, 1992) and is adequate for most uses: $\mathrm{Log}(p) = a - b/T$; *with* $a = 27.9546$ and $b = 3182.48$, p is in Pascal, T is in Kelvin.

The thermal conductivity of CO_2 gas can be fit by an empirical formulation as

$k_g = -12.0817 + 1.39898\,T$; the value is $\sim 0.006\,\mathrm{W\,s^{-1}\,m^{-1}\,K^{-1}}$ at 145 K.

Although the kinetic theory of gases yields viscosity to be proportional to $\sqrt{T}$, experimental data available over the temperature range from 190 K to 290 K (Lange, 1967; Weast, 1970) more closely follow $\nu = \exp(1.4326 + 0.004404\ T)$. The extrapolated value at 145 K is 8 μPa s.

Solid carbon dioxide at Martian pressures forms a cubic crystal lattice. The latent heat of sublimation is $6.52308 \times 10^5 - 371.28\,T\ \mathrm{J\,kg^{-1}}$.

Thermal conductivity of the solid from 120 to 150 K in $\mathrm{W\,s^{-1}\,m^{-1}\,K^{-1}}$ follows closely the equation $k = 93.4/T$ (Kravchenko and Krupskii, 1998).

The heat capacity of the solid is $459.6 + 1.3585\ T\,\mathrm{kJ\,kg^{-1}\,K^{-1}}$

The density of solid CO_2 is $1606\,\mathrm{kg\,m^{-3}}$. However, estimates of the bulk density of CO_2 ice deposits on Mars suggest a range of $\sim 600\,\mathrm{kg\,m^{-3}}$ (Haberle *et al.*, 2004) to $\sim 1000\,\mathrm{kg\,m^{-3}}$ (Smith *et al.*, 2001a; Prettyman *et al.*, 2004).

REFERENCES

Aharonson, O., M. T. Zuber, D. E. Smith, *et al.*, Depth, distribution, and density of CO_2 deposition on Mars, *J. Geophys. Res.* **109**, E05004, doi:10.1029/2003JE002223, 2004.

Antoniadi, E. M., 1930, *The Planet Mars*, Trans. Patrick Moore, Devon, UK: Keith Reid Ltd., 1975.

Barker, E. S., R. A. Schorn, A. Woszczyk, R. G. Tull, and S. J. Little, Mars: detection of atmospheric water vapor during the southern hemisphere spring and summer season, *Science* **170**, 1308–10, 1970.

Bass, D. S., K. E. Herkenhoff, and D. A. Paige, Variability of Mars' north polar water ice cap. 1. Analysis of Mariner 9 and Viking Orbiter imaging data, *Icarus* **144**, 382–96, 2000.

Basu, S., M. I. Richardson, and J. R. Wilson, Simulation of the Martian dust cycle with the GFDL Mars GCM, *J. Geophys. Res.* **109**, E11006, doi:10.1029/2004JE002243, 2004.

Bell III, J. F., P. C. Thomas, M. J. Wolff, S. W. Lee, and P. B. James, Mineralogy of the north polar sand sea from 1995 Hubble Space Telescope near-IR observations. *Lunar Planet. Sci. Conf. XXVIII*, Abstract #1757, 1997.

Bell, J. F., H. Y. McSween, J. A. Crisp, *et al.*, Mineralogic and compositional properties of Martian soil and dust: results from Mars Pathfinder, *J. Geophys. Res.* **105**, 1721–55, 2000.

Benson, J. L. and P. B. James, Yearly comparisons of the martian polar caps: 1999–2003 Mars Orbiter Camera observations, *Icarus* **174**, 513–23, 2005.

Bibring, J.-P., Y. Langevin, F. Poulet, *et al.*, Perennial water ice identified in the South polar cap of Mars, *Nature* **428**, 627–30, 2004.

Bonev, B. P., P. B. James, J. E. Bjorkman, and M. J. Wolff, Regression of the Mountains of Mitchel polar ice after the onset of a global dust storm on Mars, *Geophys. Res. Lett.* **29**, doi:10.1029/2002GL015458, 2002.

Bonev, B. P., J. E. Bjorkman, G. B. Hansen, P. B. James, and M. J. Wolff, Effects of atmospheric dust on residual south polar cap stability, *Annu. Lunar Planet. Conf. XXXVI*, Houston, TX: Lunar and Planetary Institute, Abstract #1101, March 14–18, 2005.

Boynton, W., W. C. Feldman, S. W. Squyres, *et al.*, Distribution of hydrogen in the near surface of Mars: evidence for subsurface ice deposits, *Science* **297**, 81–5, 2002.

Byrne, S. and A. P. Ingersoll, A sublimation model for Martian south polar ice features, *Science* **299**, 1051–3, 2003.

Calvin, W. M., Additions and corrections to the absorption coefficients of CO_2 ice: applications to the martian south polar cap, *J. Geophys. Res.* **95**, 14743–50, 1990.

Calvin, W. M. and T. N. Titus, Summer season variability of the north residual cap of Mars as observed by the Mars Global Surveyor Thermal Emission Spectrometer (MGS-TES), *Planet. Space Sci.*, in press, doi:10.1016/j.pss.2007.08.005, 2007. AQ4

Cantor, B., M. Malin, and K. S. Edgett, Multiyear Mars Orbiter Camera (MOC) observations of repeated Martian weather phenomena during the northern summer season, *J. Geophys. Res.* **107**, CiteID 5014, doi:10.1029/2001JE001588, 2002.

Clancy, R. T., S. W. Lee, G. R. Gladstone, W. W. McMillan, and T. Roush, A new model for Mars atmospheric dust based upon analysis of ultraviolet through infrared observations from Mariner 9, Viking, and Phobos, *J. Geophys. Res.* **100**, 5251–63, 1995.

Clancy, R. T., M. J. Wolff, and P. R. Christiansen, Mars aerosol studies with the MGS TES emission phase function observations: Opacities, particle sizes, and ice cloud types versus latitude and solar longitude, *J. Geophys. Res.* **108**, 5098, doi:10.1029/2003JE002058, 2003.

Colaprete, A., R. M. Haberle, and O. B. Toon, Formation of convective carbon dioxide clouds near the south pole of Mars, *J. Geophys. Res.* **108**, CiteID 5081, doi:10.1029/2003JE002053, 2003.

Colaprete, A., J. R. Barnes, R. M. Haberle, *et al.*, Albedo of the south pole on Mars determined by topographic forcing of atmosphere dynamics, *Nature* **435**, 184–8, 2005.

Colaprete, A., J. R. Barnes, R. M. Haberle, and F. Montmessin, CO_2 clouds, CAPE and convection on Mars: observations and general circulation modeling, *Planet. Space Sci.*, in press, doi:10.1016/j.pss.2007.08.010, 2007. AQ5

Cutts, J. A. and R. S. U. Smith, Eolian deposits and dunes on Mars, *J. Geophys. Res.* **78**, 4139–54, 1973.

Cutts, J. A., K. R. Blasius, G. A. Briggs, *et al.*, North polar region of Mars: imaging results from Viking 2, *Science* **194**, 1329–37, 1976.

Douté, S., B. Schmitt, Y. Langevin, J. -P. Bibring, *et al.*, South pole of Mars: nature and composition of the icy terrains from Mars Express OMEGA observations, *Planet. Space Sci.* **55**, 113–33, 2007.

Durham, W. B., S. H. Kirby, and L. A. Stern, Creep of water ices at planetary conditions: a compilation, *J. Geophys. Res.* **102**, 16293–302, 1997.

Durham, W. B., S. H. Kirby, and L. A. Stern, Steady-state flow of solid CO_2: preliminary results, *Geophys. Res. Lett.* **26**, 3493–6, 1999.

Farmer, C. B., D. W. Davies, and D. D. LaPorte, Mars: northern summer ice cap water vapor observations from Viking 2, *Science* **194**, 1339–41, 1976.

Feldman, W. C., T. H. Prettyman, W. V. Boynton, *et al.*, CO_2 frost cap thickness on Mars during northern winter and spring, *J. Geophys. Res.* **108**, CiteID 5103, doi:10.1029/2003JE002101, 2003.

Feldman, W. C., T. H. Prettyman, S. Maurice, *et al.*, Global distribution of near-surface hydrogen on Mars, *J. Geophys. Res.* **109**, CiteID E09006, doi:10.1029/2003JE002160, 2004.

Fischbacher, G. E., L. J. Martin, and W. A. Baum, *Martian Polar Cap Boundaries*. Final Report A, Contract 951547, Jet Propulsion Laboratory, Pasadena, CA. Planetary Research Center, Lowell Observatory, Flagstaff, AZ, 1969.

Fisher, D. A., Internal layers in an "accublation" ice cap: a test for flow, *Icarus* **144**, 289–94, 2000.

Folkner, W. M., R. D. Kahn, R. A. Preston, *et al.*, Mars dynamics from Earth-based tracking of the Mars Pathfinder lander, *J. Geophys. Res.* **102**, 4057–64, 1997.

Forget, F. and J. B. Pollack, Thermal infrared observations of the condensing Martian polar caps: CO_2 ice temperatures and radiative budget, *J. Geophys. Res.* **101**, 16865–79, 1996.

Forget, F., G. B. Hansen, and J. B. Pollack, Low brightness temperatures of Martian polar caps: CO_2 clouds or low surface emissivity, *J. Geophys. Res.* **100**, 21219–34, 1995.

Forget, F., F. Hourdin, and O. Talagrand, CO_2 snowfall on Mars: simulation with a general circulation model, *Icarus* **131**, 302–16, 1998.

Forget, F., F. Hourdin, R. Fournier, *et al.*, Improved general circulation models of the Martian atmosphere from the surface to above 80 km, *J. Geophys. Res.* 104, 24155–76, 1999.

Glenar, D. A., G. Hansen, G. Bjoraker, *et al.*, Bright-region radiative properties within the Mars south polar cap ($L_s = 231°$) from near-infrared spectroscopic imaging, *Icarus* **174**, 600–3, 2005.

Grundy, W. M. and B. Schmitt, The temperature-dependent near-infrared absorption spectrum of hexagonal H_2O ice, *J. Geophys. Res.* **103**, 25809–22, 1998.

Grundy, W. M., M. W. Buie, J. A. Stansberry, J. R. Spencer, and B. Schmitt, Near-infrared spectra of icy outer Solar System surfaces: remote determination of H_2O ice temperatures, *Icarus* **142**, 536–49, 1999.

Haberle, R. M., M. M. Joshi, J. R. Murphy, *et al.*, General circulation model simulations of the Mars Pathfinder atmospheric structure investigation/meteorology data, *J. Geophys. Res.* **104**, 8957–74, 1999.

Haberle, R. M., B. Mattingly, and T. N. Titus, Reconciling different observations of the CO_2 ice mass loading of the Martian north polar cap, *Geophys. Res. Lett.* **31**, CiteID L05702, 2004.

Hansen, G. B., The infrared absorption spectrum of carbon dioxide ice from 1.8 to 333 micrometers, *J. Geophys. Res.* **102**, 21569–87, 1997.

Hansen, G. B., Control of the radiative behavior of the Martian polar caps by surface CO_2 ice: evidence from Mars Global Surveyor measurements, *J. Geophys. Res.* **104**, 16471–86, 1999.

Hansen, G. B., Ultraviolet to near-infrared absorption spectrum of carbon dioxide ice from 0.174 to 1.8 μm, *J. Geophys. Res.* **110**, CiteID E11003, doi:10.1029/2005JE002531, 2005.

Hansen, G. B., W. Giuranna, V. Formisano, *et al.*, PFS-MEX observation of ices in the residual south polar cap of Mars, *Planet. Space Sci.* **53**, 1089–95, 2005.

Haas, W. H., Flashes on Mars observed in 1937 and some random remarks, *J. Assoc. Lunar Planet. Observers, The Strolling Astronomer* **45**, 43–5, 2003.

Herkenhoff, K. E. and A. R. Vasavada, Dark material in the polar layered deposits and dunes on Mars, *J. Geophys. Res.* **104**, 16487–500, 1999.

Herkenhoff, K. E., S. Byrne, and K. L. Tanaka, Mars polar geologic nomenclature: what are the caps? *4th Int. Conf. Mars Polar Sci. Explor.*, Davos, Switzerland, LPI Contribution No. 1323, p. 8034, October 2–6, 2006.

Herr, K. C. and G. C. Pimentel, Infrared absorptions near 3 microns recorded over the polar cap of Mars, *Science* **166**, 496–9, 1969.

Herschel, W., On the remarkable appearances at the polar regions of the planet mars, the inclination of its axis, the position of its poles, and its spheroidical figure; with a few hints relating to its real diameter and atmosphere, *Philos. Trans. R. Soc. Lond.* **74**, 233–73, 1784.

Hess, S. L., Static stability and thermal wind in an atmosphere of variable composition: application to Mars, *J. Geophys. Res.* 84, 2969–73, 1979.

Hinson, D. P. and R. J. Wilson, Transient eddies in the southern hemisphere of Mars *Geophys. Res. Lett.* **29**, CiteID 1154, doi:10.1029/2001GL014103, 2002.

Hobbs, P. V., *Ice Physics*, Oxford: Clarendon Press, 837pp., 1974.

Houben, H., R. M. Haberle, R. E. Young, and A. P. Zent, Modeling the Martian seasonal water cycle, *J. Geophys. Res.* **102**, 9069–84, 1997.

Hourdin, F., F. Forget, and O. Talagrand, The sensitivity of the Martian surface pressure and atmospheric mass budget to various parameters: a comparison between numerical simulations and Viking observations, *J. Geophys. Res.* **100**, 5501–23, 1995.

Howard, A. D., The role of eolian processes in forming surface features of the martian polar layered deposits, *Icarus* **144**, 267–88, 2000.

Hunt, G. E., On the infrared radiative properties of CO_2 ice clouds: application to Mars, *Geophys. Res. Lett.* **7**, 481–4, 1980.

Ivanov, A. B. and D. O. Muhleman, The role of sublimation for the formation of the northern ice cap: results from the Mars Observer Laser Altimeter, *Icarus* **144**, 436–8, 2000.

Ivanov, A. B. and D. O. Muhleman, Cloud reflection observations: results from the Mars Orbiter Laser Altimeter, *Icarus* **154**, 190–206, 2001.

Jakosky, B. M., The role of seasonal reservoirs in the Mars water cycle: 1. Seasonal exchange of water with the regolith, *Icarus* **55**, 1–18, 1983a.

Jakosky, B. M., The role of seasonal reservoirs in the Mars water cycle: 2. Coupled models of the regolith, the polar caps, and atmospheric transport, *Icarus* **55**, 19–39, 1983b.

Jakosky, B. M., The seasonal cycle of water on Mars, *Space Sci. Rev.* **41**, 131–200, 1985.

Jakosky, B. M. and R. M. Haberle, Year-to-year instability of the Mars south polar cap, *J. Geophys. Res.* **95**, 1359–65, 1990.

Jakosky, B. M. and R. M. Haberle, The seasonal behavior of water on Mars. In *Mars* (ed. H. H. Kieffer *et al.*), University of Arizina Press, pp. 969–1016, 1992.

Jakosky, B. M., A. P. Zent, and R. W. Zurek, The Mars water cycle: determining the role of exchange with the regolith, *Icarus* **130**, 87–95, 1997.

James, P. B., H. H. Kieffer, and D. A. Paige, Seasonal cycle of carbon dioxide on Mars. In *Mars* (ed. H. H. Kieffer *et al.*), University of Arizona Press, pp. 934–68, 1992.

James, P. B., B. P. Bonev, and M. J. Wolff, Visible albedo of Mars' south polar cap: 2003 HST observations, *Icarus* **174**, 596–9, 2005.

Jones, K. L., R. E. Arvidson, E. A. Guinness, *et al.*, One Mars year: Viking lander imaging observations, *Science* **204**, 799–806, 1979.

Kahn, R., T. Z. Martin, R. W. Zurek, and S. W. Lee, The Martian dust cycle. In *Mars* (ed. H. H. Kieffer *et al.*), University of Arizona Press, pp. 1017–53, 1992.

Kahre, M. A., J. R. Murphy, and R. M. Haberle, Modeling the Martian dust cycle and surface dust reservoirs with the NASA Ames general circulation model, *J. Geophys. Res.* **111**, E06008, doi:10.1029/2005JE002588, 2006.

Kelly, N. J., W. V. Boynton, K. Kerry, *et al.*, Seasonal polar carbon dioxide frost on Mars: CO_2 mass and columnar thickness distribution, *J. Geophys. Res.* **111**, E03S07, doi:10.1029/2006JE002678, 2006.

Kieffer, H. H., Mars south polar spring and summer temperatures: A residual CO_2 frost, *J. Geophys. Res.* **84**, 8263–88, 1979.

Kieffer, H. H., H_2O grain-size and the amount of dust in Mars residual north polar-cap, *J. Geophys. Res.* **95**, 1481–93, 1990.

Kieffer, H. H., Cold jets in the martian polar caps, *J. Geophys. Res.* **112**, E08005, doi:10.1029/2006JE002816, 2007.

Kieffer, H. H. and T. Titus, TES mapping of Mars' north seasonal cap, *Icarus* **154**, 162–80, 2001.

Kieffer, H. H., S. C. Chase Jr., T. Z. Martin, E. D. Miner, and F. D. Palluconi, Martian north pole summer temperatures: dirty water ice, *Science* **194**, 1341–4, 1976.

Kieffer, H. H., T. N. Titus, K. F. Mullins, and P. R. Christensen, Mars south polar spring and summer behavior observed by TES: seasonal cap evolution controlled by frost grain size, *J. Geophys. Res.* **105**, 9653–99, 2000.

Kieffer, H. H., P. R. Christensen, and T. N. Titus, CO_2 jets formed by sublimation beneath translucent slab ice in Mars' seasonal south polar ice cap, *Nature* **442**, 793–6, 2006.

Kravchenko, Y. and I. Krupskii, Thermal conductivity of solid N_2O and CO_2, *Sov. J. Low Temp. Phys.* **12**, 46–8, 1998.

Lancaster, N. and R. Greeley, Sediment volume in the north polar sand sea of Mars, *J. Geophys. Res.* **95**, 10921–7, 1990.

Lange, N. A., *Lange's Handbook of Chemistry*, 10th edn., revised. New York: McGraw-Hill, 1967

Langevin, Y., F. Poulet, J.-P. Bibring, *et al.*, Summer evolution of the north polar cap of Mars as observed by OMEGA/Mars Express, *Science* 307, 1581–3, 2005.

Langevin, Y., S. Douté, M. Vincendon, *et al.*, No signature of clear CO_2 ice from the "cryptic" regions in Mars' south seasonal cap, *Nature* **442**, 790–2, 2006.

Langevin, Y., J.-P. Bibring, F. Montmessin, *et al.*, Observations of the south seasonal cap of Mars during recession in 2004–2006 by the OMEGA visible/near-infrared imaging spectrometer on board Mars Express, *J. Geophys. Res.* **112**, E08S12, doi:10.1029/2006JE002841, 2007.

Larson, H. P. and U. Fink, Identification of carbon dioxide on the Martian polar caps, *Astrophys. J.* **171**, L91–L95, 1972.

Lemmon, M. T., M. J. Wolff, M. D. Smith, *et al.*, Atmospheric imaging results from the Mars exploration rovers: Spirit and opportunity, *Science* **306**, 1753–6, 2004.

Leighton, R. R. and B. C. Murray, Behavior of carbon dioxide and other volatiles on Mars, *Science* **153**, 136–44, 1966.

Litvak, M. L., I. G. Mitrofanov, A. S. Kozyrev, *et al.*, Long-term observations of southern winters on Mars: estimations of column thickness, mass, and volume density of the seasonal CO_2 deposit from HEND/Odyssey data, *J. Geophys. Res.* **112**, E03S13, doi:10.1029/2006JE002832, 2007.

Malin, M. C., M. H. Carr, G. E. Danielson, *et al.*, Early views of the Martian surface from the Mars orbiter camera of Mars global surveyor, *Science* **279**, 1681–5, 1998.

Malin, M. C., M. A. Caplinger, and S. D. Davis, Observational evidence for an active surface reservoir of solid carbon dioxide on Mars, *Science* **294**, 2146–8, 2001.

Markiewicz, W. J., R. M. Sablotny, H. U. Keller, *et al.*, Optical properties of the Martian aerosols as derived from Imager for Mars Pathfinder midday sky brightness data, *J. Geophys. Res.* **104**, 9009–17, 1999.

Martin, L. J., P. B. James, A. Dollfus, K. Iwasaki, and J. D. Beish, Telescopic observations: visual, photographic, polarimetric. In *Mars* (ed. H. H. Kieffer *et al.*), Tucson: University of Arizona Press, pp. 34–70, 1992.

Montmessin, F., F. Forget, P. Rannou, M. Cabane, and R. M. Haberle, Origin and role of water ice clouds in the Martian water cycle as inferred from a general circulation model, *J. Geophys. Res.* **109**, E10004, doi:10.1029/2004JE002284, 2004.

Montmessin, F., J. L. Bertaux, E. Quemerais, *et al.*, Subvisible CO_2 ice clouds detected in the mesosphere of Mars, *Icarus* **183**, 403–10, 2006.

Neugebauer, G., G. Miinch, H. H. Kieffer, S. C. Chase Jr., and E. Miner, Mariner, 1969 Infrared Radiometer results: temperatures and thermal properties of the martian surface, *Astron. J.* **76**, 719, 1971.

Neumann, G. A., D. E. Smith, and M. T. Zuber, Two Mars years of clouds detected by Mars Orbiter Laser Altimeter, *J. Geophys. Res.* **108**, doi:10.1029/2002JE001849, 2003.

Nye, J. F., W. B. Durham, P. M. Schenk, and J. M. Moore, The instability of a south polar cap on Mars composed of carbon dioxide, *Icarus* **144**, 449–55, 2000.

Ockert-Bell, M. E., J. F. Bell, J. B. Pollack, C. P. McKay, and F. Forget, Absorption and scattering properties of the Martian dust in the solar wavelengths, *J. Geophys. Res.* **102**, 9039–50, 1997.

Paige, D. A., The annual heat balance of the Martian polar caps from Viking observations, Ph.D. thesis, California Institute of Technology, 1985.

Paige, D. A. and A. P. Ingersoll, Annual heat-balance of Martian polar caps: Viking observations, *Science* **228**, 1160–8, 1985.

Paige, D. A. and K. D. Keegan, Thermal and albedo mapping of the polar regions of Mars using Viking thermal mapper observations. 2. South polar region, *J. Geophys. Res.* **99**, 25993–26013, 1994.

Paige, D. A., J. E. Bachman, and K. D. Keegan, Thermal and albedo mapping of the polar regions of Mars using Viking thermal mapper observations: 1. North polar region, *J. Geophys. Res.* **99**, 25959–91, 1994.

Pearl, J. C., M. D. Smith, B. J. Conrath, and P. R. Christensen, Observations of Martian ice clouds by the Mars Global Surveyor Thermal Emission Spectrometer, *J. Geophys. Res.* **106**, 12325–38, 2001.

Piqueux, S., S. Byrne, and M. I. Richardson, Sublimation of Mars's southern seasonal CO_2 ice cap and the formation of spiders, *J. Geophys. Res.* **108**, CiteID 5084, doi:10.1029/2002JE002007, 2003.

Pollack, J. B., R. M. Haberle, J. R. Murphy, J. Schaeffer, and H. Lee, Simulations of the general circulation of the Martian atmosphere: 2. Seasonal pressure variations, *J. Geophys. Res.* **98**, 3149–81, 1993.

Pollack, J. B., M. E. Ockert-Bell, and M. K. Shepard, Viking lander image analysis of Mar, tian atmospheric dust, *J. Geophys. Res.* **100**, 5235–50, 1995.

Prettyman, T. H., W. C. Feldman, M. T. Mellon, *et al.*, Composition and structure of the Martian surface at high southern latitudes from neutron spectroscopy, *J. Geophys. Res.* **109**, E05001, doi:10.1029/2003JE002139, 2004.

Prettyman, T. H., R. C. Elphic, W. C. Feldman, *et al.*, Spatial deconvolution of Mars Odyssey neutron spectroscopy data: analysis of Mars southern seasonal cap, *Lunar Planet. Sci. XXXVI*, Abstract #1384, 2005.

Quirico, E. and B. Schmitt, Near-infrared spectroscopy of simple hydrocarbons and carbon oxides diluted in solid N_2 and as pure ices: implications for Triton and Pluto, *Icarus* **127**, 354–78, 1997.

Richardson, M. I. and R. J. Wilson, Investigation of the nature and stability of the Martian seasonal water cycle with a general circulation model, *J. Geophys. Res.* **107**, 5031, doi:10.1029/2001JE001536, 2002.

Roach, L. H., J. F. Mustard, S. Murchie, *et al.*, CRISM spectral signatures of the north polar gypsum dunes, *Lunar Planet. Sci.*

Conf. XXXVIII, League City, Texas, LPI Contribution No. 1338, p. 1970, March 12–16, 2007.

Schmitt, B., S. Douté, Y. Langevin, *et al.*, *Northern seasonal condensates on Mars by OMEGA/Mars Express, Annu. Lunar Planet. Sci. Conf. XXXVI*, League City, Texas, Abstract #2326, March 14–18, 2005a.

Schmitt, B., S. Douté, Y. Langevin, *et al.*, Spring sublimation of the seasonal condensates on Mars from OMEGA/Mars Express, *Fall AGU Meeting*, Abstract #P23C-02, 2005b.

Smith, D. E., M. T. Zuber, and G. A. Neumann, Seasonal variations of snow depth on Mars, *Science* **294**, 2141–6, 2001a.

Smith, D. E., M. T. Zuber, H. V. Frey, *et al.*, Mars Orbiter Laser Altimeter: experiment summary after the first year of global mapping of Mars, *J. Geophys. Res.* **106**, 23689–722, 2001b.

Smith, D. E., M. T. Zuber, Variation in the masses of the seasonal martian icecaps, Fall AGU Meeting, Abstract #P23C-01, 2005.

Smith, M., Interannual variability in TES atmospheric observations of Mars during 1999–2003, *Icarus* **167**, 148–65, 2004.

Soderblom, L. A., M. C. Malin, J. A. Cutts, and B. C. Murray, Mariner 9 observations of the surface of Mars in the north polar region, *J. Geophys. Res.* **78**, 4197–210, 1973.

Sprague, A. L., W. V. Boynton, K. E. Kerry, *et al.*, Mars' south polar Ar enhancement: a tracer for south polar seasonal meridional mixing, *Science* **306**, 1364–7, 2004.

Stoney, G. Jo, Of atmospheres upon planets and satellites, *Astrophys. J.* **7**, **25**, 1898.

Svitek, T. and B. Murray, Winter frost at Viking Lander 2 site, *J. Geophys. Res.* **95**, 1495–510, 1990.

Tanaka, K. L. and D. H. Scott, Geologic map of the polar regions of Mars, Scale 1:15,000,000. *USGS Misc. Inv. Ser. Map*, I-1802 C, 1987.

Thomas, P., K. E. Herkenhoff, A. D. Howard, B. C. Murray, and S. L. Squyres, Polar deposits of Mars. In *Mars* (ed. H. H. Kieffer *et al.*), University of Arizona Press, pp. 767–95, 1992.

Thomas, P. C., M. C. Malin, K. S. Edgett, *et al.*, North-south geological difference between the residual polar caps on Mars, *Nature* **404**, 161–4, 2000.

Thomas, P. C., M. C. Malin, P. B. James, *et al.*, South polar residual cap of Mars: features, stratigraphy, and changes, *Icarus* **174**, 535–59, 2005.

Tillman, J. E., N. C. Johnson, P. Guttorp, and D. B. Percival, The Martian annual atmospheric-pressure cycle: years without great dust storms, *J. Geophys. Res.* **98**, 10963–71, 1993.

Titov, D. V., Water Vapour in the atmosphere of Mars, *Adv. Space. Res.* **29**, 183–91, 2002.

Tinus, T. N. and H. H. Kieffer, IR spectral properties of dust and ice at the mass south polar cap, American Astronomical society, DPS Meeting #33, Abstract #19.15, *Bull. Am. Astrom.* **33**, 1071, 2001.

Titus, T. N., Mars polar cap edges tracked over 3 full Mars years, *Annu. Lunar Planet. Sci. Conf. XXXVI*, Houston, TX: Lunar and planetary Institute, Abstract #1993, March 14–18, 2005a.

Titus, T. N., Thermal infrared and visual observations of a water ice lag in the Mars southern summer, *Geophys. Res. Lett.* **32**, L24204, doi:10.1029/2005GL024211, 2005b.

Titus, T. N., Kieffer, H. H., Mullins, K. F., TES observations of the south pole, American Astronomical Society, DPS meeting #30, #20.05, *Bull. Amer. Astron. Soc.* **30**, 1049, 1998.

Titus, T., H. H. Kieffer, K. F. Mullins, and P. R. Christensen, TES premapping data: slab ice and snow flurries in the Martian north polar night, *J. Geophys. Res.* **106**, 23181–96, 2001.

Titus, T. N., H. H. Kieffer, and P. R. Christensen, Exposed water ice discovered near the south pole of Mars, *Science* **299**, 1048–51, 2003.

Tokar, R. L., W. C. Feldman, T. H. Prettyman, *et al.*, Ice concentration and distribution near the south pole of Mars: synthesis of Odyssey and global surveyor analyses, *Geophys. Res. Lett.* **29**, 1904, doi:10.1029/2002GL015691, 2002.

Tomasko, M. G., L. R. Doose, M. Lemmon, P. H. Smith, and E. Wegryn, Properties of dust in the Martian atmosphere from the Imager on Mars Pathfinder, *J. Geophys. Res.* **104**, 8987–9007, 1999.

Tsoar, H., R. Greeley, and A. R. Peterfreund, Mars: the north polar sand sea and related wind patterns, *J. Geophys. Res.* **84**, 8167–80, 1979.

Tyler, D. and J. R. Barnes, A mesoscale model study of summertime atmospheric circulations in the north polar region of Mars, *J. Geophys. Res.* **110**, CiteID E06007, doi:10.1029/2004JE002356, 2005.

Tyler, G. L., G. Balmino, D. P. Hinson, *et al.*, Radio science observations with Mars Global Surveyor: orbit insertion through one Mars year in mapping orbit, *J. Geophys. Res.* **106**, 23327–48, 2001.

Wagstaff, K. L., T. N. Titus, and A. B. Ivanov, R. Castaño, and J. L. Baudfield, Observations of the north polar water ice annulus on Mars using THEMIS and TES, *Planet. Space Sci.*, in press, doi:10.1016/j.pss.2007.08.008, 2007. AQ6

Wall, S. D., Analysis of condensates formed at the Viking-2 Lander site: the 1st winter, *Icarus* **47**, 173–83, 1981.

Ward, W. R. and D. J. Rudy, Resonant obliquity of Mars? *Icarus* **94**, 160–4, 1991.

Wang, H. and A. P. Ingersoll, Martian clouds observed by Mars Global Surveyor Mars Orbiter Camera, *J. Geophys. Res.* **107**, CiteID 5078, doi:10.1029/2001JE001815, 2002.

Warren, S. G., Optical constants of ice from the ultraviolet to the microwave, *Appl. Opt.* **23**, 1206–25, 1984.

Weast, R. C. (ed.), *Handbook of Chemistry and Physics*, 51st edn., Cleveland: Chemical Rubber Co., 1970.

Wells, E. H. and D. P. Hale, Flashes on Mars observed in 1937 and some random remarks, *Nature* **232**, 324–5, 1971.

Wilson, L. J., Apparent flashes seen on Mars, *Pop. Astron.* **45**, 430, 1937.

Winfree, K. W. and T. N. Titus, Estimation of CO_2 coverage on Mars' south pole: an interannual assessment, *Annu. Lunar Planet. Sci. Conf. XXXVII, League City, Texas*, Abstract #2283, March 13–17, 2006.

Wolff, M. J. and R. T. Clancy, Constraints on the size of Martian aerosols from Thermal Emission Spectrometer observations, *J. Geophys. Res.* **108**, 5097, doi:10.1029/2003JE002057, 2003.

Wolff, M. J., M. D. Smith, R. T. Clancy, *et al.*, Constraints on dust aerosols from the Mars Exploration Rovers using MGS overflights and Mini-TES, *J. Geophys. Res.* **111**, E12S17, doi:10.1029/2006JE002786, 2006.

Yoder, C. F. and E. M. Standish, Martian precession and rotation from Viking lander range data, *J. Geophys. Res.* **102**, 4065–80, 1997.

Zasova, L., V. Formisano, V. Moroz, *et al.*, Water clouds and dust aerosols observations with PFS MEX at Mars, *Planet. Space Sci.* **53**, 1065–77, 2005.

Zuber, M. T., D. E. Smith, S. C. Soloman, *et al.*, Observations of the north polar region of Mars from the Mars Observer Laser Altimeter, *Science* **282**, 2053–60, 1998.

Author Query for Chapter 25:

AQ1: “Smith 2002 is not listed in references. Please check.

AQ2: “Kieffer mass, finding” has been changed to Kieffer mass, not only finding…” As this OK?

AQ3: “Blunck 1982” is not listed in references. Please check.

AQ4: Please update – in press.

AQ5: Please update – in press.

AQ6: Please update – in press.